Worldline and Worldsheet Techniques in Lattice Field Theory

New algorithmic developments for worldline representations of lattice field theories with fermions

Oliver Orasch[1]

in collaboration with Shailesh Chandrasekharan[2] and Christof Gattringer[3]

Table of Contents

[1] University of Graz, Institute of Physics,Universitätsplatz 5, 8010 Graz, Austria (oliver.orasch@uni-graz.at)
[2] Duke University, Physics Department, Box 90305, 27708 Durham, NC, USA
[3] University of Graz, Institute of Physics, Universitätsplatz 5, 8010 Graz, Austria

1 Introduction

Ab-initio calculations are key to understanding the non-perturbative aspects of particle, nulcear and condensed matter physics. One method where non-perturbative physics is accessible is lattice field theory which is heavily based on Markov Chain Monte Carlo techniques and, thus, requires smart algorithms and powerful machines. Lattice calculations usually make use of the path integral formalism where each configuration is weighted by a Boltzmann factor $\exp(-S[C])$ containing the classical action of the system. Then, the quantum nature arises from the summation over all possible states C. If $S \in \mathbb{R}$, each state appears with probability $\exp(-S[C])/Z$ where Z is an appropriate normalization factor called partition sum. Then, we may use importance sampling to generate configurations C and measure observables.
However, there are cases where $S \in \mathbb{C}$, and a probability interpretation of $\exp(-S[C])/Z$ is not possible. As a result, strong oscillations of the integrand occur and importance sampling techniques become inefficient or simply fail. These cases are said to be plagued by sign problems, or more generally, complex action problems which appear in many theories of interest in condensed matter, nuclear and particle physics. Sign problems are not restricted to Lagrangian methods, i.e., methods using path integral quantization, they also appear in Hamiltonian systems where canonical quantization is employed. In some sense, sign problems are a common feature of many complex or strongly correlated multi-particle systems of both relativistic and non-relativistic nature. The most (in)famous sign problems arise from real time, the Pauli exclusion principle [1], finite density [2], a topological charge [3], or frustration of quantum spins [4]; but there are many more. Thus, to study such systems it is necessary to understand and control sign problems. A limiting factor to that effort is the fact that sign problems are assumed to be NP-hard [1], meaning that there is no generic solution and each case has to be analyzed independently. Furthermore, the severity of sign problems strongly depends on the representation, e.g., by changing the representation one might even induce a sign problem. Over the last couple of decades many strategies have been proposed to attenuate/circumvent/avoid sign problems: worldline methods [5], stochastic quantization [6], reweighting [7], canonical methods [8], or density of states [9] to name a few.
In this work, we use worldline methods which arise from integrating out the original degrees of freedom, i.e., matter and/or gauge fields. By doing so, we exactly map the system to a statistical system of integer occupation numbers. To be more precise, we focus on fermionic worldline systems. Generically, such systems are plagued by the fermion sign problem which arises from the Pauli exclusion principle.
In the first chapter, we study the massless Schwinger model in two dimensions. For this model the sign problem is completely solved by a worldline representation. However, we focus on yet another aspect of the Pauli principle: The stiffness of worldline simulations due to Pauli blocking. We show that summing up all configurations with the same fermion loop structure is possible, at the cost of introducing an auxiliary bosonic field with non-local weights called “Path Activation Determinants”. We stress that the considerations are merely of algorithmic nature.
In the second chapter, we revisit the idea of worldline simulations of strong coupling QCD. There, we use a fermion bag strategy to solve the fermion sign problem. We introduce the representation and propose a local algorithm to update the configurations. Furthermore, we try to motivate that the fraction of the lattice that is occupied by the bag, i.e., the bag size, is an interesting observable. The latter is a measure for the worldline degrees of freedom. The main question we want to address: Which worldline degrees of freedom are dominant? Surely, the answer will depend on whether chiral symmetry is broken or not. In this work, however, we only consider a two-dimensional system where the Mermin-Wagner theorem [10] forbids spontaneous breaking of a continuous symmetry. Thus, this work is understood as a proof-of-principle study and a test bed for simulations in four dimensions. Additionally, we propose a novel worm algorithm to cross-check the simulations using the bag partition sum on small lattices and to study the chiral limit (this is unfortunately not possible with our current local algorithm).
To conclude, we want to stress that this work explores re-summation techniques in the context of fermion worldline simulations. This is possible since the degrees of freedom are discrete, and, hence, we can systematically group large sets of worldline configurations.

2 Path Activation Determinants

As a result of the Pauli exclusion principle, it is numerically very hard to study fermions. In standard simulations the fermion determinant needs to be computed, and in worldline representations one needs to take care of the fermion sign problem. Furthermore, the Pauli principle states that two fermions with the same quantum numbers cannot occupy the same space-time point. This gives rise to extremely stiff fermion worldline systems which are hard to update with a local algorithm (Pauli blocking). Stiff systems often give rise to long auto-correlation times which means that measurements of observables in a Monte Carlo simulation need to be separated sufficiently.
In this work, we propose a new approach to deal with stiff system of worldlines. The strategy is to sum up large sets of configurations into so-called „Path Activation Determinants“ which we abbreviate as PADs in the rest of the text. The main idea is to consider dimer configurations for a fixed loop structure. Interestingly, it is possible to sum up all dimer configurations compatible with a certain loop configuration, giving rise to non-local weights.

2.1 The massless Schwinger model with a Vacuum term

The Schwinger model is QED in two dimensions. It is an interesting toy model for QCD as it shares common features such as confinement and asymptotic freedom. Thus, it is an interesting test bed for algorithmic ideas.

The partition function for this model is given by

$$Z = \int \mathcal{D}[U]\mathcal{D}[\overline{\psi},\psi] e^{-S_G[U] - i\theta Q[U] + S_F[U,\overline{\psi},\psi]}, \tag{2.1}$$

where U denotes configurations of the group valued U(1) link variables. The ψ and $\overline{\psi}$ are 1-component Grassmann fields for the fermions. The fermion fields live on a lattice with N_s sites in the spatial direction and N_t sites in temporal direction. In the following, we use an index that labels all the sites $x = 0, \ldots, V-1$ $(V = N_s N_t)$ and a directional index $\nu = 1, 2$ (or other greek letters). Hence, the combination of (x, ν) labels a link. For the gauge fields (which live on the links), we use periodic boundary conditions in both space and time direction. However, for the fermions we choose the boundary conditions to be anti-periodic in temporal direction and periodic in space.

The U(1) gauge field $U_{x,\nu}$ is related to the continuum field $A_{x,\nu}$ (the corresponding Lie algebra) by

$$U_{x,\nu} = \exp(iA_{x,\nu}) \;\text{ with }\; A_{x,\nu} \in [-\pi, \pi]. \tag{2.2}$$

The integration measures appearing in (2.1) are products of U(1) Haar measures and Grassmann measures

$$\int \mathcal{D}[U] = \prod_{x,\nu} \int_{-\pi}^{\pi} \frac{\mathrm{d}A_{x,\nu}}{2\pi} \;,\; \int \mathcal{D}[\overline{\psi}\psi] = \prod_x \int \mathrm{d}\overline{\psi}_x \mathrm{d}\psi_x. \tag{2.3}$$

We use the Wilson gauge action

$$S_G[U] = -\beta \sum_x \mathrm{Re}\, U_p(x), \tag{2.4}$$

where the sum runs over all plaquettes $U_p(x)$ which are defined as

$$U_p(x) = U_{x,1} U_{x+\hat{1},2} U^{\dagger}_{x+\hat{2},1} U^{\dagger}_{x,2}. \tag{2.5}$$

We also include a topological charge $Q[U]$ which couples to a θ-angle giving rise to a sign problem in the conventional representation. On the lattice a possible discretization of the topological charge is

$$Q[U] = \frac{1}{2\pi} \sum_x \mathrm{Im}\ U_p(x). \tag{2.6}$$

It is straightforward to show that the continuum version of the topological charge is recovered in the naive continuum limit.

The last ingredient that is missing is the lattice fermion action. We use the massless staggered action with one flavor of fermions

$$S_F[U, \overline{\psi}, \psi] = \frac{1}{2} \sum_x \sum_\nu \gamma_{x,\nu} [\overline{\psi}_x U_\nu(x) \psi_{x+\hat{\nu}} - \overline{\psi}_{x+\hat{\nu}} U_\nu^\dagger(x) \psi_x], \tag{2.7}$$

where the $\gamma_{x,\nu}$ is the staggered sign function. In two dimensions, $\gamma_{x,\nu}$ is given by

$$\gamma_{x,1} = 1\ ,\ \gamma_{x,2} = (-1)^{x_1}. \tag{2.8}$$

Usually, mass terms of the type $m\overline{\psi}_x\psi_x$ appear in the action. However, we consider only the massless case since the presence of mass terms give rise to a severe fermion sign problem in the worldline formulation that will be introduced in the next section.

2.1.1 Solving the Sign problem: Worldline representation

As it stands, the partition function (2.1) is not suitable for Monte Carlo simulation. The fermions can be integrated out which gives rise to a real and positive fermion determinant and, thus, fermions do not pose an immediate threat to numerical fantasies of the author. The topological charge, however, couples to $i\theta$ and, thus, gives rise to a sign problem in the conventional formulation.
In [11] the authors present a method to map the Schwinger model to a statistical system of worldlines and worldsheets. The matter degrees of freedom, i.e., the worldlines, are fermion loops and dimers. Fermion loops, as the name suggests, are the fermionic degrees of freedom since each loop carries a sign that only depends on geometrical properties of the loop itself. The sign is the implementation of the Pauli principle and, thus, an important aspect of fermion physics. Apparently, this sign is always positive if the system is free of on-site terms called monomers, i.e., mass terms, and, thus, we restrict this discussion to the $m = 0$ case. Apart from fermion loops which are closed, non-intersecting hops of fermions, the worldline system also includes dimers. The latter are formed by a forward fermion hop and an immediate backward hop on the same link, i.e., $\overline{\psi}_x\psi_{x+\hat{\nu}}\overline{\psi}_{x+\hat{\nu}}\psi_x$. Since a dimer does not carry a sign, it is said to be bosonic. The gauge degrees of freedom (worldsheets) in the worldline representation are plaquette occupation numbers which occupy hypersurfaces on the lattice.
Interestingly, it is also possible to a add topological charge to the system and still solve the complex action problem in the worldline representation [12]. Due to the special structure of the discretization of the topological charge (2.6) it is also possible to integrate out the gauge field in the case $\theta \neq 0$ and, thus, obtain a worldline representation with real and positive weights.

In the following, we will shortly summarize the worldline/worldsheet representation given in [11,12] for the massless Schwinger model. Usually, worldline representations are obtained by integrating out the conventional degrees of freedom. This is a map from Grassmann/complex valued degrees of freedom to (usually) integer valued degrees of freedom. We start with expanding the exponential function $\exp(S_F[U, \overline{\psi}, \psi])$

$$
\begin{aligned}
\mathrm{e}^{S_F[\bar{\psi},\psi,U]} &= \prod_{x,\nu} e^{\frac{\gamma_\nu(x)}{2}\bar{\psi}(x)U_\nu(x)\psi(x+\hat{\nu})} e^{-\frac{\gamma_\nu(x)}{2}\bar{\psi}(x+\hat{\nu})U_\nu^*(x)\psi(x)} \\
&= \prod_{x,\nu} \sum_{\ell_{x,\nu}=0}^{1} \left(\frac{\gamma_\nu(x)}{2}\bar{\psi}(x)U_\nu(x)\psi(x+\hat{\nu})\right)^{\ell_{x,\nu}} \times \\
&\qquad \sum_{\bar{\ell}_{x,\nu}=0}^{1} \left(-\frac{\gamma_\nu(x)}{2}\bar{\psi}(x+\hat{\nu})U_\nu^*(x)\psi(x)\right)^{\bar{\ell}_{x,\nu}}.
\end{aligned}
\tag{2.9}
$$

Due to the nilpotency of the Grassmann numbers, the expansion terminates after the first order. In this form the Grassmann integration can be performed.
For a configuration to have non-vanishing weight it must saturate the Grassmann integral on every site

$$
\prod_x \int \mathrm{d}\psi_x \mathrm{d}\overline{\psi}_x \overline{\psi}_x \psi_x = 1. \tag{2.10}
$$

The latter simply states that every site x has to be occupied by one bilinear $\overline{\psi}_x\psi_x$. According to Equation (2.9), the lattice can now be filled with dimers and loops. The latter are formed by consecutive $\ell_{x,\nu} = 1$ and $\bar{\ell}_{x,\nu} = 1$ that form closed non-self-intersecting contours. Each loop contributes with

$$
\left(\frac{1}{2}\right)^{|L|} \mathrm{sign}(L) \Big(\prod_{(x,\nu)\in L} U_{x,\nu} \Big) \prod_{i=1}^{|L|} \bar{\psi}(x_i)\psi(x_i), \tag{2.11}
$$

where $|L|$ denotes the total length of a loop L. The sign of a loop is written as $\mathrm{sign}(L)$ and it is given by

$$
\mathrm{sign}(L) = -(-)^{|L|/2}(-)^{w[L]}(-)^{P[L]}. \tag{2.12}
$$

The sign is composed of four individual signs: the overall sign arises from the rearranging of Grassmann variables to the canonical order, the second sign takes into account all hoppings in negative direction (compare with the staggered action (2.7) where every backward hop has a minus sign), the third sign reflects the total number of temporal windings ($w[L]$ is the temporal winding number; Gauss law requires $w[L] = 0$) and the fourth sign stems from the staggered sign functions ($P[L]$ denotes the number of plaquettes enclosed by the loop). As it turns out, the massless lattice Schwinger model in a worldline representation is free of the fermion sign problem and

$$
\mathrm{sign}(L) = +1 \quad \forall\, L. \tag{2.13}
$$

This can be traced back to the fact that without monomers, i.e., isolated sites, $|L|/2 + P[L]$ is always odd. Additionally, the Grassmann integral can be satisfied with dimers, i.e., $\ell_{x,\nu} = 1$ and $\bar{\ell}_{x,\nu} = 1$. In the partition sum the dimers appears with

$$
\frac{1}{4}\bar{\psi}(x)\psi(x)\bar{\psi}(x+\hat{\nu})\psi(x+\hat{\nu}). \tag{2.14}
$$

After the Grassmann integration, the integral over the gauge field can easily be performed. For this step, we first need to treat the exponential containing the gauge action and the topological charge

$$
\begin{aligned}
\mathrm{e}^{-S_G[U]-i\theta\mathrm{Q}[U]} &= \prod_x e^{\eta U_p(x)}\ e^{\bar{\eta}U_p^*(x)} \\
&= \prod_x \sum_{p_x\in\mathbb{Z}} I_{|p_x|}(2\sqrt{\eta\bar{\eta}}) \left(\frac{\eta}{\bar{\eta}}\right)^{\frac{p_x}{2}} U_p(x)^{p_x}.
\end{aligned}
\tag{2.15}
$$

In the first line, we collected the contributions from the gauge action and the topological charge. For convenience, we define a new set of parameters η and $\bar{\eta}$ which are related to the original parameters (β, θ) in the following way

$$\eta = \beta/2 - \theta/4\pi \ , \ \bar{\eta} = \beta/2 + \theta/4\pi. \tag{2.16}$$

To obtain the result in the second line of Equation (2.15), the exponentials in the first line need to be expanded in a power series. After some rearranging and algebraic considerations, it becomes obvious that the plaquettes factor out and the rest sums up to modified Bessel functions of the first kind, as shown above. The new expansion index p_x is called the plaquette occupation number and represents the gauge field as a worldsheet. p_x refers to the plaquette defined by the sites $x,\ x+\hat{1},\ x+\hat{1}+\hat{2}$ and $x+\hat{2}$.

The form of (2.15) makes it easy to integrate out the gauge field since all integrals are of the type

$$\int_{U(1)} \mathcal{D}[U] U^j = \delta(j), \tag{2.17}$$

where the $\delta(j)$ is the Kronecker delta. In the language of worldlines, a Kronecker delta imposes a constraint on the wordline/worldsheet configurations. To be more precise, the integration of the gauge field gives rise to the following constraints

$$C[\mathcal{L}, p] \equiv \prod_x \delta(\ell_{x,1} - \bar{\ell}_{x,1} + p_x - p_{x-\hat{2}}) \delta(\ell_{x,2} - \bar{\ell}_{x,2} - p_x + p_{x-\hat{1}}), \tag{2.18}$$

where $\mathcal{L}$ is an arbitrary loop configuration, i.e., a collection of fermion loops L defined by values of $\ell_{x,\nu}$ and $\bar{\ell}_{x,\nu}$ such that occupied $\ell_{x,\nu}$ and $\bar{\ell}_{x,\nu}$ form closed loops including dimers. p simply denotes a worldsheet configuration. Since in the constraint (2.18) only differences of $\ell_{x,\nu}$ and $\bar{\ell}_{x,\nu}$ appear, it is natural to define a new variable

$$k_{x,\nu} \equiv \ell_{x,\nu} - \bar{\ell}_{x,\nu} = 1, 0, -1. \tag{2.19}$$

Since $k_{x,\nu} = 0$ if a link is occupied by a dimer or not occupied at all, $k_{x,\nu}$ is understood as a flux variable for the fermion loops. If $k_{x,\nu} = 1$ a loop exits site x in positive direction, if $k_{x,\nu} = -1$ a loop exits site x in negative direction.
The meaning of the constraint $C[\mathcal{L}, p]$ is the following: Each flux $k_{x,\nu}$ needs to be compensated by flux stemming from the occupation of the plaquettes that share the link (x, ν). Together with the Grassmann constraint, i.e., the requirement that fermion worldlines must close and are not allowed to intersect, this means that plaquette occupation numbers can be non-zero if the area defined by this occupation is bounded by a fermion loop. Thus, $C[\mathcal{L}, p]$ and the Grassmann constraint implement the Gauss law. The latter requires that the total winding number of fermion loops $w[L]$ vanishes. Additionally, (2.18) allows for constant non-zero plaquette occupation, i.e., $p_x = p \ \forall x$.

As mentioned above there is an ambiguity for the $k_{x,\nu} = 0$ case. To get rid of the latter, we also define a dimer occupation number which is given by

$$d_{x,\nu} = \ell_{x,\nu} \bar{\ell}_{x,\nu}. \tag{2.20}$$

Putting all the ingredients together, we arrive at the following form of the partition sum of the massless Schwinger model in a worldline representation

$$Z = \left(\frac{1}{2}\right)^V \sum_{\{\mathcal{L},d,p\}} \left[\prod_x I_{|p_x|}(2\sqrt{\eta\bar{\eta}})\left(\frac{\eta}{\bar{\eta}}\right)^{\frac{p_x}{2}}\right] C[\mathcal{L},p], \tag{2.21}$$

where the sum runs over configurations of loops $\mathcal{L}$ (encoded by occupations of k variables), dimers d, and plaquettes p. The constant up front stems from the weights of the fermion hops, i.e., $1/2$: Since the lattice is completely filled with loops and dimers, the overall amount of factors of $1/2$ (weight of one loop element) and $1/4 = (1/2)^2$ (weight of a dimer) sums exactly up to V. If we choose $\beta > |\theta|/2\pi$, then all weights in (2.21) are real and positive and the sign problem is gone.

Since we can drop the constant in the partition function, the fermion worldlines (loops and dimers) have weight 1. However, the fermion loops are accompanied by occupied plaquettes which in turn carry the weights shown in parenthesis in Equation (2.21). So, if we design an algorithm for a Monte Carlo simulation, there will be an accept-reject-step necessary to check if a move is possible or not. For the dimers, however, no such step is necessary since all dimer configurations compatible with a loop configuration have weight 1. The main purpose of a dimer update is to sample configurations of equal weight. As it turns out, a non-local worm update is needed for the job [12,13]. Since the dimers just present an unimportant background for the loop configuration, one may ask if it is possible to sum up all dimer configurations compatible with the latter. This leads to the concept of Path Activation Determinants.

2.1.2 Path Activation Determinants

We start by writing the partition function (2.1) as

$$Z = \int \mathcal{D}[U] e^{-S_G[U] - i\theta Q[U]} Z_F[U], \tag{2.22}$$

where $Z_F[U]$ is the fermion partition function for a fixed gauge field configuration U. Above, we have seen that the latter may be written as

$$Z_F[U] = \sum_{\{\mathcal{L}\}} \left[\prod_{L\in\mathcal{L}} \left(\frac{1}{2}\right)^{|L|} \Big(\prod_{(x,\nu)\in L} U_{x,\nu}\Big)\right] W[\mathcal{L}], \tag{2.23}$$

where $W[\mathcal{L}]$ is the weight factor for the dimer configuration. It takes into account all possible dimer configurations compatible with $\mathcal{L}$, i.e.,

$$W[\mathcal{L}] = \sum_{\{d||\mathcal{L}\}} \left(\frac{1}{4}\right)^{N_d}, \tag{2.24}$$

where N_d is simply the total number of dimers. In contrast to (2.21), we explicitly do not make use of the fact that

$$\sum_{L\in\mathcal{L}} |L| + 2N_d = V. \tag{2.25}$$

In an attempt to sum up all the dimer configurations compatible with a given $\mathcal{L}$, we write a path integral

$$W[\mathcal{L}] = \int \mathcal{D}[\bar{\psi},\psi]\; e^{S_{\mathcal{L}}[\bar{\psi},\psi]}, \tag{2.26}$$

where we introduced a model action $S_{\mathcal{L}}[\overline{\psi},\psi]$.

It is given by

$$S_{\mathcal{L}}[\overline{\psi},\psi] = \sum_x [1-\xi_x]\overline{\psi}_x\psi_x + \frac{1}{4}\sum_\nu \overline{\psi}_x\psi_x\overline{\psi}_{x+\hat{\nu}}\psi_{x+\hat{\nu}}\xi_x\xi_{x+\hat{\nu}}. \tag{2.27}$$

Note that the index x runs over all the lattice sites and not only over the domains occupied by dimers in (2.24). To correct for that, it is necessary to introduce variable ξ_x that is used for bookkeeping which links are occupied by loops. It is defined as

$$\xi_x = \begin{cases} 0 & \text{for } x \in L,\ \forall L \in \mathcal{L} \\ 1 & \text{otherwise} \end{cases}. \tag{2.28}$$

This means that if a site is occupied by a loop $\xi_x = 0$, and only the diagonal term in (2.27) appears. If, however, a site x and some adjacent site $x+\hat{\nu}$ are not occupied by a loop, then it is possible to occupy the respective link with a dimer and the contribution is off-diagonal.
Since we made up a model action, it is not easy to collectively integrate out the Grassmann valued fermion fields. To do s,o, we need to massage the dimer weight a little bit further.

More specifically, we will break up the quartic dimer term in (2.26)

$$e^{\frac{1}{4}\overline{\psi}_x\psi_x\overline{\psi}_{x+\hat{\nu}}\psi_{x+\hat{\nu}}\xi_x\xi_{x+\hat{\nu}}} = 1 - \frac{1}{4}\overline{\psi}_x\psi_{x+\hat{\nu}}\xi_x\xi_{x+\hat{\nu}}\overline{\psi}_{x+\hat{\nu}}\psi_x\xi_x\xi_{x+\hat{\nu}}. \tag{2.29}$$

The first step towards breaking up the term was already executed in the last equation: Since the ξ_x are binary, it is also possible to use ξ_x^2 instead. Furthermore, we notice that the quartic dimer factor has a strong resemblance with 4-Fermi interaction terms. Usually, such terms are treated with a Hubbard-Stratonovich transformation. Here, we use a discrete version of the latter to break up the quartic term into bilinear terms, at the cost of introducing an auxiliary field $\sigma_{x,\nu}$

$$\begin{gathered} 1 - \frac{1}{4}\overline{\psi}_x\psi_{x+\hat{\nu}}\xi_x\xi_{x+\hat{\nu}}\overline{\psi}_{x+\hat{\nu}}\psi_x\xi_x\xi_{x+\hat{\nu}} = \\ \sum_{\sigma_{x,\nu}=\pm 1}\left(1+\frac{1}{2}\overline{\psi}_x\psi_{x+\hat{\nu}}\xi_x\xi_{x+\hat{\nu}}\sigma_{x,\nu}\right)\left(1-\frac{1}{2}\overline{\psi}_{x+\hat{\nu}}\psi_x\xi_x\xi_{x+\hat{\nu}}\sigma_{x,\nu}\right) = \\ \sum_{\sigma_{x,\nu}=\pm 1} e^{\frac{1}{2}\overline{\psi}_x\psi_{x+\hat{\nu}}\xi_x\xi_{x+\hat{\nu}}\sigma_{x,\nu}}\ e^{-\frac{1}{2}\overline{\psi}_{x+\hat{\nu}}\psi_x\xi_x\xi_{x+\hat{\nu}}\sigma_{x,\nu}}. \end{gathered} \tag{2.30}$$

In the last line of Equation (2.30), we used the Grassmann nature of the fermion fields to write the expressions in parentheses as the respective exponential function. By introducing the auxiliary field $\sigma_{x,\nu}$, we can write (2.26) with a bilinear expressions

$$W[\mathcal{L}] = \left(\frac{1}{2}\right)^{2V}\prod_{x,\nu}\sum_{\sigma_{x,\nu}=\pm 1}\int \mathcal{D}[\bar{\psi},\psi]e^{\sum\limits_{x,y}\overline{\psi}_x M_{x,y}(\sigma,\mathcal{L})\psi_y}, \tag{2.31}$$

where the matrix M is given by

$$M_{x,y}(\sigma,\mathcal{L}) = [1-\xi_x]\delta_{x,y} + \frac{1}{2}\sum_\nu[\delta_{x+\hat{\nu},y}\sigma_{x,\nu}\xi_x\xi_y - \delta_{x-\hat{\nu},y}\sigma_{y,\nu}\xi_x\xi_y]. \tag{2.32}$$

The matrix can be understood in such a way that it has only non-vanishing diagonal elements if a specific site is occupied by a loop. If, however, two adjacent sites are not occupied by a loop, then it is possible to

place a dimer, and these elements are filled with the auxiliary field. Why this is useful, we can see by carrying out the Grassmann integration in (2.31)

$$W[\mathcal{L}] = \left(\frac{1}{2}\right)^{2V} \sum_{\{\sigma\}} \det M(\sigma, \mathcal{L}), \tag{2.33}$$

where we introduced the sum over all configurations of the auxiliary variables, $\sum_{\{\sigma\}} = \prod_{x,\nu} \sum_{\sigma_{x,\nu}=\pm 1}$. Note that here we simply summed up large sets of dimer configurations. The loops and the gauge field are not affected by that at all. Therefore, it is possible to carry out the integration of the gauge field as described in the previous section. Making use of Equation (2.33), the full partition function with PADs is given by

$$Z = \sum_{\{\mathcal{L},p,\sigma\}} \left[\prod_{L\in\mathcal{L}} \left(\frac{1}{2}\right)^{|L|}\right] \det M(\sigma,\mathcal{L}) \left[\prod_x I_{|p_x|}(2\sqrt{\eta\bar{\eta}}) \left(\frac{\eta}{\bar{\eta}}\right)^{\frac{p_x}{2}}\right] C[\mathcal{L},p], \tag{2.34}$$

where we dropped the overall constant appearing in (2.33). Since the fermion loop structure is imprinted in the matrices $M(\sigma,\mathcal{L})$, the determinants of the latter are denoted as “Path Activation Determinants”.

Finally, it is necessary to show that the partition function (2.34) is again free of a sign problem. Since the weights for the loops and the plaquettes are obviously real and positive (as argued in the previous section), it is sufficient to show that the same holds for the determinant of $M(\sigma,\mathcal{L})$. Consider a fixed loop configuration $\mathcal{L}$ and a fixed configuration of the auxiliary field σ, i.e.,

$$\begin{aligned} \det M(\sigma,\mathcal{L}) = \int \mathcal{D}[\bar{\psi},\psi] \prod_x \left(1 + (1-\xi_x)\overline{\psi}_x\psi_x\right) \times \\ \prod_{x,\nu} \left(1 + \tfrac{1}{2}\overline{\psi}_x\psi_{x+\hat{\nu}}\xi_x\xi_{x+\hat{\nu}}\sigma_{x,\nu}\right) \times \\ \prod_{x,\nu} \left(1 - \tfrac{1}{2}\overline{\psi}_{x+\hat{\nu}}\psi_x\xi_x\xi_{x+\hat{\nu}}\sigma_{x,\nu}\right), \end{aligned} \tag{2.35}$$

where we expanded each exponential function. Interestingly, it is now possible to use the same language we used to make sense of Equation (2.9). By construction, the first line incorporates the structure of the loops in the original loop configuration $\mathcal{L}$, the second and third line resemble hopping terms (in the original staggered action (2.9)) coupling to an external field σ. Due to this resemblance, we again obtain dimers and loops coupling to σ. In terms of worldlines, we write (2.35) as

$$\det M(\sigma,\mathcal{L}) = \sum_{\{\mathcal{L}',d'\}} \left(\frac{1}{4}\right)^{N_{d'}} \prod_{L'\in\mathcal{L}'} \left(\frac{1}{2}\right)^{|L'|} \mathrm{sign}(L') \prod_{(x,\nu)\in L'} \sigma_{x,\nu}. \tag{2.36}$$

The first thing we note is that

$$\mathrm{sign}(L') \prod_{(x,\nu)\in L'} \sigma_{x,\nu} = \pm 1, \tag{2.37}$$

which means that every loop (we already take into account both orientations) and the contributions from the auxiliary file have a combined weight of

$$\pm \left(\frac{1}{2}\right)^{|L'|} \times\ 2. \tag{2.38}$$

Suppose, we replace the loop by a chain of dimers. Due to the Grassmann constraint, the contour previously occupied by the loop can be filled with $|L'|/2$ dimers. Additionally, it is possible to fill the links along the contour in two ways. Thus, the weight of the corresponding dimer chain is given by

$$+\left(\frac{1}{2}\right)^{|L'|} \times 2. \tag{2.39}$$

Combining (2.38) and (2.39) yields

$$\det M(\sigma, \mathcal{L}) \geq 0. \tag{2.40}$$

2.1.3 Algorithm

To update the system, we use three distinct Monte Carlo updates: (i) Loop updates, (ii) blanket updates for the gauge field and (iii) updates for the auxiliary field.

(i) The loop updates try to alter the loop configuration. This can be achieved by creating a loop, deleting a loop, growing a loop, shrinking a loop, merging two loops into a single loop or separating a single loop into two loops. Before we define the updates, it is worthwhile to examine the smallest fermion loop possible, a 1×1-loop around a plaquette. Every loop can be thought of as a superposition of the latter. Thus, to create a loop we simply check for empty plaquettes and try to put a 1×1-loop there. The orientation is chosen by tossing a coin. Thus, to satisfy detailed balance we only decide to delete 1×1-loops with a probability of $1/2$. Growing and shrinking of a loop works quite similar: If we scan the lattice and encounter a loop segment, the algorithm tries to enlarge the area enclosed by the loop by adding flux around the adjacent plaquette. Again, to respect detailed balance the shrinking of a loop is exactly opposite to the growing move. Lastly, we can also include a merging and separating of loops. In some cases it is possible to rotate two loop segments around a plaquette. If it is possible, such a move may merge loops or separate a loop. As mentioned earlier, the loops carry the weights of the plaquette occupations within a loop, and changing the local loop configurations yields a change in the plaquette occupation by ± 1. Therefore, the accept-reject-rate is given by

$$\rho_{\mathcal{L}} = \left(\frac{1}{2}\right)^{\Delta L} \left(\sqrt{\frac{\eta}{\overline{\eta}}}\right)^{\pm 1} \frac{I_{|p_x \pm 1|}\left(2\sqrt{\eta\overline{\eta}}\right)}{I_{|p_x|}\left(2\sqrt{\eta\overline{\eta}}\right)} \frac{\det M\left(\sigma, \mathcal{L}'\right)}{\det M\left(\sigma, \mathcal{L}\right)} \tag{2.41}$$

where ΔL is the change in the loop length. In the fashion of the Metropolis algorithm, the moves are accepted with the probability $\min\left(1, \rho_{\mathcal{L}}\right)$. Finally, it is interesting to point out the difference of the dimer-free-formulation with PADs to the formulation with dimers: To respect the Grassmann constraint, it is necessary to replace loop segments with dimers in the original worldline formulation and vice versa. This is important for the growing move where we need to have a dimer on the link facing the link we want to change. This is not necessary in the PAD formulation.

(ii) Since the constraint (2.18) also allows for constant non-zero plaquette occupation, we also define blanket updates which simply raise/lower all plaquette occupation numbers p_x by ± 1. Again, the accept-reject-rate is built up by ratio of Bessel functions and square root factors containing η and $\overline{\eta}$. Since all plaquettes get changed simultaneously, a product over all the lattice sites needs to be taken, i.e.,

$$\rho_p = \left(\sqrt{\frac{\eta}{\overline{\eta}}}\right)^{\pm V} \prod_x \frac{I_{|p_x \pm 1|}\left(2\sqrt{\eta\overline{\eta}}\right)}{I_{|p_x|}\left(2\sqrt{\eta\overline{\eta}}\right)}. \tag{2.42}$$

This move is also accepted with $\min\left(1, \rho_p\right)$.

(iii) Since no constraint needs to be respected, the auxiliary field σ is fairly easy to update. We simply try to flip $+1$ to -1 and vice versa. The accept-reject-rate is then given by ratios of PADs,

$$\rho_\sigma = \frac{\det M\left(\sigma', \mathcal{L}\right)}{\det M\left(\sigma, \mathcal{L}\right)}. \tag{2.43}$$

Again, this move is accepted with $\min\left(1, \rho_\sigma\right)$.

At the end, we would like to comment on the ratios of PADs. Usually (in case of updates of worldline configurations), it is possible to relate the ratios of fermion determinants to the matrix elements of the inverse fermion matrix which is numerically cheaper to evaluate [5]. This is possible by utilizing the nilpotency property of the Grassmann numbers in the respective path integral. In the case of the massless Schwinger model, however, this is not possible since $M(\sigma, \mathcal{L})$ may have zero modes, and, thus, in some cases it may not be invertible (see (2.40)).

2.1.4 Observables

For a proof-of-concept study, we measure two observables: the plaquette expectation value and the topological charge density. The former is defined by a β-derivative and the latter by a θ-derivative of $\ln Z$, i.e.,

$$\langle U_p \rangle = \frac{1}{V}\frac{\partial}{\partial\beta}\ln Z \qquad \text{and} \qquad \langle q \rangle = -\frac{1}{V}\frac{\partial}{\partial\theta}\ln Z. \tag{2.44}$$

Using the worldline partition function (2.34), the expectation value of the plaquette is given by

$$\langle U_p \rangle = \frac{1}{V}\left\langle \sum_x \frac{\partial_\beta I_{|p_x|}\left(2\sqrt{\eta\overline{\eta}}\right)}{I_{|p_x|}\left(2\sqrt{\eta\overline{\eta}}\right)} + \frac{p_x}{4}\left(\frac{1}{\eta} - \frac{1}{\overline{\eta}}\right)\right\rangle. \tag{2.45}$$

The topological charge, on the other hand, is

$$\langle q \rangle = -\frac{1}{V}\left\langle \sum_x \frac{\partial_\theta I_{|p_x|}\left(2\sqrt{\eta\overline{\eta}}\right)}{I_{|p_x|}\left(2\sqrt{\eta\overline{\eta}}\right)} - \frac{p_x}{8\pi}\left(\frac{1}{\eta} + \frac{1}{\overline{\eta}}\right)\right\rangle. \tag{2.46}$$

To evaluate the derivative of the Bessel functions, we use a well-known property of Bessel functions,

$$\frac{\partial}{\partial x} I_n(f(x)) = \frac{1}{2}\Big[I_{n+1}(f(x)) + I_{n-1}(f(x))\Big]\frac{\partial f(x)}{\partial x}. \tag{2.47}$$

2.2 Results

For a proof-of-concept study, we provide numerical results for the plaquette expectation value and the topological charge density. We cross-check our results on a 4×4 lattice with analytical data from [12]. In the case of vanishing vacuum angle θ, we also provide data from a conventional simulation using the fermion determinant and sampling over the gauge field. Also the latter was taken from [12]. For the test simulation, we use 10^4 sweeps to equilibrate the system. After the thermalization we measure the observables 2×10^5 times intercepted by 10 decorrelation sweeps. One sweep is given by successive application of the updates defined in Section 2.1.3, i.e., the update of the fermion loops, global update of the plaquette occupations and the update of the auxiliary Hubbard-Stratonovich field.

First, we show the results for the plaquette expectation value for vanishing θ. Figure 1 shows the results

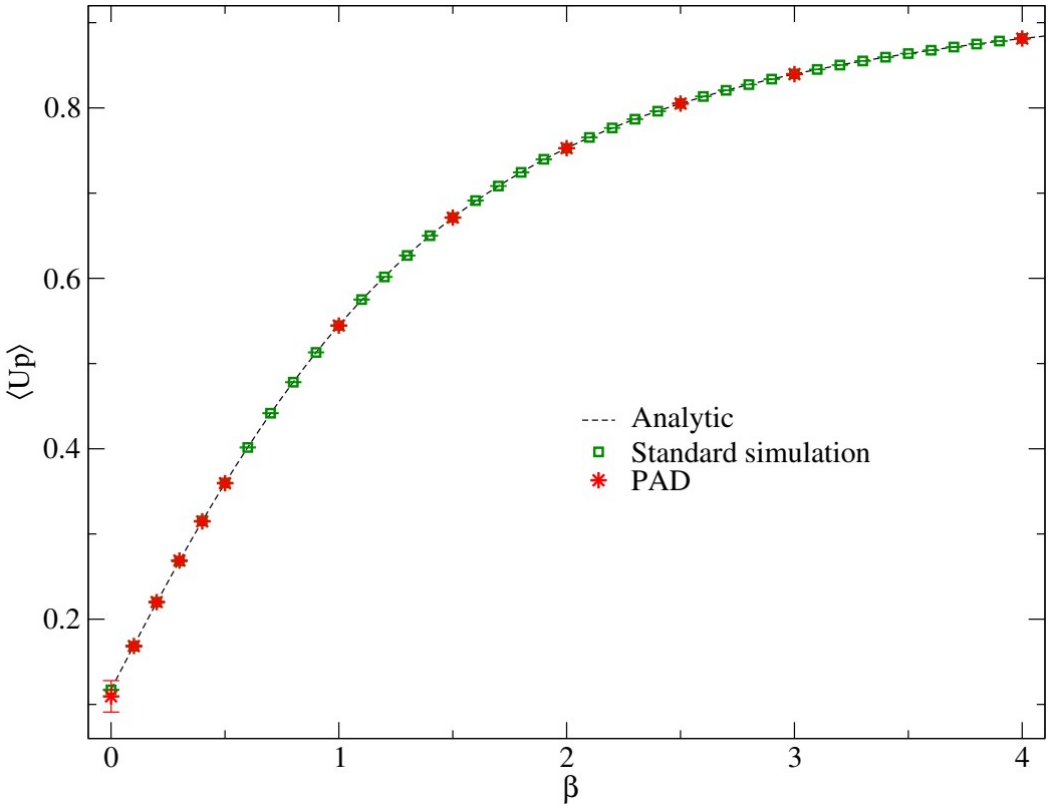

Figure 1: Plaquette expectation value as a function of the inverse gauge coupling β for $\theta = 0$. The dashed line is the analytic result obtained by β-expansion of the partition function. The order of the expansion is $\mathcal{O}(\beta^{64})$. The green squares were obtained by a conventional simulation. The red stars represent data from a worldline simulation with PADs. The reference data was taken from [12].

from the worldline simulations with the PAD approach confronted with analytic data and data from the conventional simulation. The data points are practically on top of each other and agree well within error bars. The first data point, however, shows a large error bar compared with the data points for higher β. This can be traced back to the fact that at small β, in this case $\beta = 0.0001$, it is very unlikely to place a non-vanishing plaquette occupation. But when it is possible, the contributions are extremely large, and, thus,

this imbalance of weight and probability gives large error bars. Increasing the statistics by a factor of 10 or more would cure the discrepancy.

The interesting case arises now when we take the vacuum angle θ to be non-zero. For this case the conventional algorithm cannot be used anymore since the fermion determinant develops an imaginary part. In Figure 2, we show the expectation values of the plaquette and the topological charge density as a function of θ for a fixed value of β. Again, we confront the data from the PAD simulation with analytic data. The reference data was again taken from [12]. The lattice dimension is, as before, 4×4, and the simulation parameters are as given in the previous paragraph.

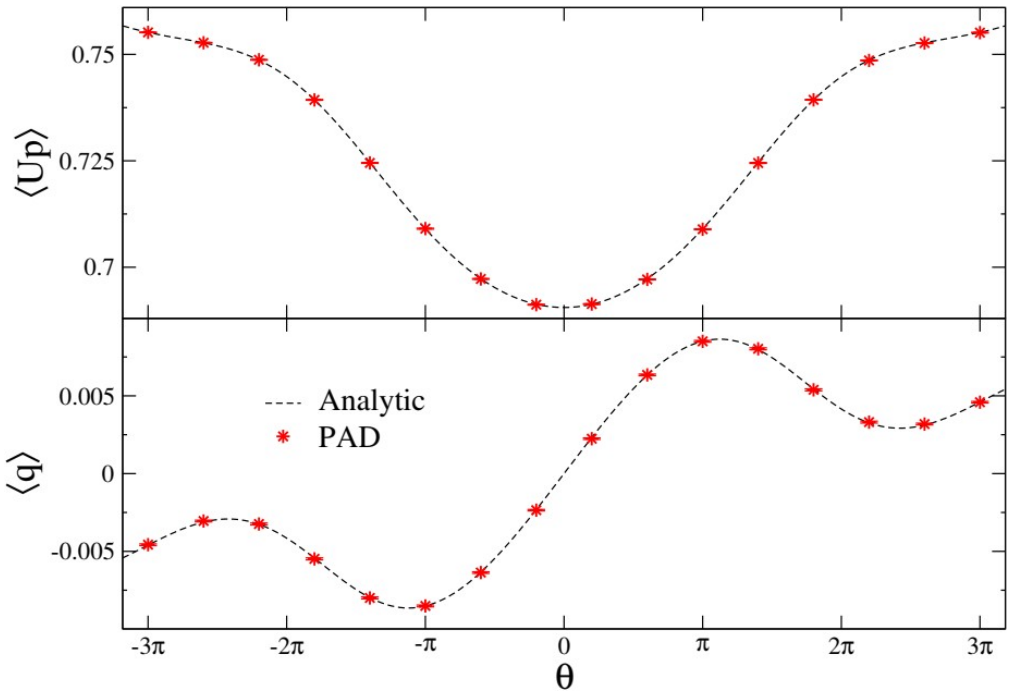

Figure 2: Expectation value of the plaquette (top) and the topological charge density (bottom) as a function of θ for $\beta = 1.6$. The red data points denote the results from the PAD worldline simulation; the dashed lines are analytic reference data taken from [12].

We clearly see, that the simulation data and the reference data are in excellent agreement, as it is the case for the data for the plaquette expectation in Figure 1. Hence, we conclude that the algorithm is implemented correctly and that the algorithm is ergodic and satisfies the detailed balance condition.

2.3 Conclusions and Outlook

In the first part of this report, we showed the construction of “Path Activation Determinants”, or PADs in short, for the case of the massless Schwinger model with a vacuum term in two dimensions. For non-vanishing θ this model has a sign problem in the conventional representation. To overcome this complex action problem, a worldline representation may be used at the cost of having a stiff system of fermion worldlines to update. The stiffness of the system arises from the fact that fermions have to obey the Pauli exclusion principle which states that each site needs to be occupied by a single fermion. Hence, global

change is not easily realized by a local algorithm. In case of worldline systems containing dimers, such as the Schwinger model discretized with staggered fermions, the dimers are subject to this issue. Apparently, a local update is not sufficient to update the dimers correctly [13]: Dimer configurations are classified by the parity of dimers living on the boundary links and a local algorithm cannot switch between those classes. In [12] a worm algorithm was used to shuffle dimer configuration. In this work we propose a different strategy to update dimers using a re-summation strategy. Re-summation of large sets of configurations may be worthwhile at the cost of computing those collective weights. The difference to a conventional method, however, is the fact that the partition function in the PAD approach is still free of a sign problem.

This report is understood as a proof-of-concept study of the PAD approach. With the results given in Section 2.2, we have shown the validity of the implementation as well as the representation. In subsequent studies, it may be interesting to show the applicability to other models also in higher dimensions. Regarding the computational effort of evaluating the PADs, it also may be worthwhile to treat the determinants further, e.g., use the PADs together with a pseudo-fermion approach. The PAD approach is understood as a trade-off of the following kind: In the original worldline formulation (2.21) the weights are local, but a non-local/worm-type algorithm is needed for ergodicity. In the PAD approach, however, the weights are maximally non-local (which is expensive), but the algorithm is local and extremely simple. For future projects it may be interesting to quantify this trade-off.

3 Baryon bags in strong coupling QCD

In recent years, a reliable determination of the μ-T phase diagram of QCD has been of great interest. See , e.g., [14] for a recent review of lattice results. Due to inefficiencies or failures of naive Monte Carlo methods, collectively denoted as sign problems, alternative approaches are needed for the task. In this work, we use a baryon bag approach to simulate strong coupling QCD along the $\mu = 0$ line. In the fermion/baryon bag approach, the fermionic degrees of freedom are confined to space-time regions called fermion/baryon bags where the physics is described by free fermions/baryons. The rest of the lattice is filled with interacting bosonic/mesonic degrees of freedom. The fermion sign problem is completely solved in this approach. As a reference, we propose a novel worm algorithm which is an upgrade of the U(3) worm introduced by Adams and Chandrasekharan [15] to non-zero quark mass.

3.1 Fermion bag approach

Fermion bags naturally appear in theories with 4-Fermi interactions. For example, consider a lattice version of the Thirring model with the action [5,16]

$$S[\overline{\psi},\psi] = \sum_{x,y} \overline{\psi}_x D_{x,y} \psi_x + \lambda \sum_{x,\nu} \overline{\psi}_{x+\hat{\nu}} \psi_{x+\hat{\nu}} \overline{\psi}_x \psi_x, \tag{3.1}$$

where $D_{x,y}$ denotes the free staggered Dirac operator. The fermion fields ψ and $\overline{\psi}$ are represented by 1-component Grassmann numbers. Thus, due to nilpotency of the latter, the only possibility to include a 4-Fermi interaction (of a single flavor of fermions) is to distribute the interaction on two adjacent sites. λ denotes the coupling strength. The partition sum for this model is then given by

$$Z = \int \prod_x \mathrm{d}\psi_x \mathrm{d}\overline{\psi}_x \exp(S). \tag{3.2}$$

Expanding only the exponentials of the interaction terms in (3.2) in a power series, we arrive at

$$\exp(S) = \exp(\overline{\psi} D \psi) \ \times \prod_{x,\nu} \sum_{d_{x,\nu}=0}^{1} \left(\lambda\, \overline{\psi}_{x+\hat{\nu}} \psi_{x+\hat{\nu}} \overline{\psi}_x \psi_x \right)^{d_{x,\nu}}, \tag{3.3}$$

where we used matrix-vector notation for the free part of the action. Due to nilpotency of the Grassmann numbers, the power series terminates after the first order. In the worldline language, the expansion index $d_{x,\nu}$ is called dimer occupation. For the Grassmann integral to give a non-vanishing contribution, we need to fill the lattice in such a way that each site x is occupied by a single bilinear term $\overline{\psi}_x \psi_x$. According to (3.3) this now may be achieved by terms stemming from the free part of the action, or with interaction terms. In other words, the Grassmann integration splits into regions where the integral is satisfied only with free fermion terms and regions where the integral is satisfied with the interaction terms. If we carry out the Grassmann integration, we obtain (3.2) in a wordline representation, i.e.,

$$Z = \sum_{\{d\}} \Big[\prod_{x,\nu} \lambda^{d_{x,\nu}} \Big] \det \tilde{D}[d] \tag{3.4}$$

where λ is the weight for each active dimer $d_{x,\nu}$. The new matrix $\tilde{D}[d]$ is identical to the free staggered Dirac operator D with the sites dropped that are occupied with dimers. Thus, for sufficiently large λ where interaction terms are abundant, the lattice decomposes into disconnected regions that are occupied by free fermion subsystems which we refer to as *fermion bags*. Therefore, $\tilde{D}[d]$ has block structure and the determinant factorizes

$$\det\tilde{D}[d] = \prod_i \det D[\mathcal{B}_i] \tag{3.5}$$

where $D[\mathcal{B}_i]$ is the staggered Dirac operator restricted to the fermion bag $\mathcal{B}_i$. Since each fermion loop in the fermion bag is paired with the corresponding dimer chain, all weights are non-negative, i.e.,

$$\det D[\mathcal{B}_i] \geq 0, \tag{3.6}$$

and the sign problem is gone. Summarizing, the fermion bag approach has been very successful in solving and/or understanding various models of interest in particle and condensed matter physics. See, e.g., [5,16-23]. In the following, we will apply the fermion bag strategy to QCD in the strong coupling limit, a non-abelian gauge theory.

3.2 QCD in the strong coupling limit

Let us briefly introduce the partition sum of strong coupling QCD. Since $\beta = 0$, there is no contribution from the gauge action, i.e.,

$$Z = \int \mathcal{D}[U]\mathcal{D}[\overline{\psi}\psi]\ \exp(S_F[\overline{\psi},\psi,U]), \tag{3.7}$$

where $S_F[\overline{\psi},\psi,U]$ is the fermion action. For the latter we use a staggered action

$$S_F\left[\overline{\psi},\psi,U\right] = \sum_x \left(2m\overline{\psi}_x\psi_x + \sum_\nu \xi_{x,\nu}\left[\mathrm{e}^{\mu\delta_{\nu,d}}\overline{\psi}_x U_{x,\nu}\psi_{x+\hat{\nu}} - \mathrm{e}^{-\mu\delta_{\nu,d}}\overline{\psi}_{x+\hat{\nu}}U^\dagger_{x,\nu}\psi_x\right]\right), \tag{3.8}$$

where m is the bare quark mass and μ is the quark chemical potential. The quark fields ψ_x and $\overline{\psi}_x$ are 3-component Grassmann vectors, each component representing a color. They live on the sites of a d-dimensional lattice of volume $V = N_s^{d-1}N_t$. The SU(3) valued gauge fields $U_{x,\nu}$ live on the links of the lattice. For the fermions, we choose periodic boundary conditions in spatial $(\nu = 1,\ldots,d-1)$ and anti-periodic boundary conditions in temporal $(\nu = d)$ direction. We take the boundary conditions of the gauge links to be periodic in all directions. Since we are interested in driving the temperature, we include an anisotropic coupling for the temporal direction. Together with the staggered sign functions, we combine the bare anisotropic coupling t and the staggered signs $\gamma_{x,\nu}$ into the link factor $\xi_{x,\nu} = t^{\delta_{\nu,\pm d}}\gamma_{x,\nu}$, where $\gamma_{x,\nu}$ is defined as usual,

$$\gamma_{x,1} = 1, \qquad \gamma_{x,2} = (-1)^{x_1}, \quad \ldots, \qquad \gamma_{x,d} = (-1)^{x_1+\cdots+x_{d-1}}. \tag{3.9}$$

Conventionally, the staggered action is defined with a factor of $1/2$ in front of the kinetic term. For convenience, however, we re-scaled the fermion fields by a factor of $\sqrt{2}$ yielding (3.8).

Let's take $\mu = 0$ for the moment. Then it is possible to show that the fermion determinant,

$$\det D[U] = \int \mathcal{D}[\overline{\psi}\psi]\ \exp(S_F[\overline{\psi},\psi,U]) = \int \mathcal{D}[\overline{\psi}\psi]\ \exp(\overline{\psi}D[U]\psi), \tag{3.10}$$

is real and non-negative. For the second equal sign, we wrote the action (3.8) as a bilinear where we use matrix vector notation for convenience. γ_5-hermiticity and the fact that the action (3.8) is chirally symmetric[4] ensure that the Dirac operator $D[U]$ solely has eigenvalues that appear in complex conjugate pairs [37]. Thus,

$$\det D[U] \geq 0. \tag{3.11}$$

[4] The staggered chiral transformations are $\chi_x \to \exp(i\theta\gamma_{5,x})\chi_x$ and $\overline{\chi}_x \to \overline{\chi}_x \exp(i\theta\gamma_{5,x})$ with $\gamma_{5,x} = (-1)^{x_1+\cdots+x_d}$.

In principle, it is also possible to include a quark chemical potential μ. In a conventional representation, however, this leads to a finite density sign problem since the fermion determinant may become negative or even complex. In a worldline representation the sign problem still persists. It is considered very mild, though [24].

3.2.1 Worldline representation

As a prerequisite, we introduce the worldline representation proposed by Karsch and Mütter [24,25] which has been very successful in studying the strong coupling phase diagram and other interesting problems. See, e.g., [26-29]. This representation we will use to produce reference data to check the simulation with baryon bags on small lattices. Once we have motivated and validated the baryon bag picture, we are going to use this representation instead to obtain results on larger lattices and to investigate the chiral limit.
Since the gauge action is missing in the partition sum (no plaquette terms), each gauge link can be integrated out independently [30-32]. Once the gauge links are integrated out, only the Grassmann integral remains. For the Grassmann integral to give a non-zero result, each lattice site x needs to be occupied by the term $\prod_{a=1}^{3} \overline{\psi}_{x,a}\psi_{x,a}$ (all three colors need to be present). This may be achieved with mass terms, hopping terms or a mixture of both. Carrying out the Grassmann integration maps the configuration of Grassmann-valued fermion fields to a worldline configuration. Mass terms are represented by monomer occupations n_x $(= 0, 1, 2, 3)$ where each monomer has a weight of $2m$. Hopping terms either contribute in the form of dimers $d_{x,\nu}$ $(= 0, 1, 2, 3)$ or as baryon loops $\ell_{x,\nu}$ $(= -1, 0, 1)$. The latter is a fermion loop, i.e., a closed, non-intersecting contour occupied by consecutive fermion hops of three quarks propagating simultaneously. In other words, integrating out the gauge fields confines the quarks to mesonic (quark, di-quark terms) and baryonic (tri-quark terms) objects. For the Grassmann integral to be satisfied, the worldline configurations need to meet the following constraint

$$n_x + \sum_{\nu} d_{x,\nu} + \sum_{\nu} \frac{3}{2}|\ell_{x,\nu}| = 3. \tag{3.12}$$

In the worldline representation, the partition sum for the system is given by

$$Z = \sum_{\{n,d,\ell\}} w_n \; w_d(t) \; w_\ell(t,\mu), \tag{3.13}$$

where we introduced the sum over all worldline configurations as

$$\sum_{\{n,d,\ell\}} = \prod_{x,\nu} \sum_{n_x=0}^{3} \sum_{d_{x,\nu}=0}^{3} \sum_{\ell_{x,\nu}=-1}^{1} . \tag{3.14}$$

The weights are given as follows [24,31]: Monomers come with a weight of $w_n = \prod_x (3!/n_x!)(2m)^{n_x}$. The combinatorical factor takes into account the color occupations. Dimers have a weight of $w_d(t) = \prod_{x,\nu}((3 - d_{x,\nu})!/(3!\, d_{x,\nu}!))t^{2\delta_{\nu,d} d_{x,\nu}}$ where t is the anisotropic coupling. Lastly, loops carry a weight of $w_\ell = \prod_\ell t^{3N_t(\ell)} \mathrm{sign}(\ell) \exp(3\mu(N_t^+(\ell) - N_t^-(\ell)))$ where $N_t^\pm(\ell)$ are the number of hops in positive/negative time direction and N_t is the sum of both. $\mathrm{sign}(\ell) = \pm 1$ is the sign of a loop. It is defined as

$$\mathrm{sign}(\ell) = -(-1)^{k+N_t^-(\ell)} \prod_{(x,\mu)\in\ell} \gamma_{x,\mu}, \tag{3.15}$$

where only the geometry of the contour enters. The sign is composed in the following way: The overall sign arises from bringing the Grassmann variables into the canonical order. The backward hops $N_t^-(\ell)$ and the winding number k of worldlines contribute with a sign each. Lastly, we pick up staggered signs from both the forward and backward hops.

Since the fermion loops carry a sign, the partition function (3.13) is not suitable for Monte Carlo simulations. Therefore, Karsch and Mütter proposed to simulate a U(3) system instead and appropriately reweight each configuration to SU(3). Since SU(3) and U(3) merely differ in the presence of fermion loops, the strategy is to identify closed ...-1-2-1-… dimer chains in the U(3) configuration, and superpose those chains with a fermions loop to obtain non-negative weights. Thus, SU(3) expectation values are given by

$$\langle \mathcal{O} \rangle_{SU(3)} = \frac{\left\langle \mathcal{O} \prod_\ell \left[1 + f_\ell(t) \mathrm{sign}(\ell)\right] \right\rangle_{U(3)}}{\left\langle \prod_\ell \left[1 + f_\ell(t) \mathrm{sign}(\ell)\right] \right\rangle_{U(3)}}, \tag{3.16}$$

where $f_\ell(t) = 2/(t^{n_t^\ell} + t^{-n_t^\ell})$ with $n_t^\ell = 3N_t^\ell - 2N_{Dt}^\ell$ [25]. N_t^ℓ is the number of loop segments and N_{Dt}^ℓ is the number of dimers in time direction. In the following, we propose a novel worm algorithm to update the U(3) configurations. It is an extension of the well-known U(3) worm proposed by Adams and Chandrasekharan [15] to $m \neq 0$.

3.2.2 U(3) Worm algorithm

This algorithm is designed to sample U(N) configurations. The worldline partition function for that system is given by

$$Z = \sum_{\{n,d,\ell\}} \prod_x \frac{N!}{n_x!} (2m)^{n_x} \prod_{x,\nu} \frac{(N - d_{x,\nu})!}{N!\, d_{x,\nu}!}, \tag{3.17}$$

where the occupation numbers of monomers and dimers range from 0 to N. Then, the Grassmann constraint is simply given by

$$n_x + \sum_\nu d_{x,\nu} = N. \tag{3.18}$$

The two observables of interest, in a study of the phase diagram, are the chiral condensate and the chiral susceptibility. Both observables signal the breaking of chiral symmetry. In the worldline representation, the chiral condensate is given by the monomer density, i.e.,

$$\langle \overline{\psi}\psi \rangle = \frac{1}{V} \frac{\partial}{\partial(2m)} \ln Z = \frac{1}{V(2m)} \Big\langle \sum_x n_x \Big\rangle. \tag{3.19}$$

Since m appears in the denominator, the case $m = 0$ cannot be studied directly. Thus, Adams and Chandrasekharan [15] proposed a non-local worm algorithm which is defined in such a way that m can be exactly 0. The worm is very efficient, and, hence, we extend it to operate also at $m \neq 0$.

To define the worm, it is convenient to distinguish two sets of configurations: C^0 configurations will have weights according to (3.17), C^1 denotes the *worm sector*. Configurations in C^1 have almost the same weight as configurations in C^0, apart from the fact that we introduce a *head*. The *head* of the worm may be understood as a monomer with an altered weight. The weight of a C^1 configuration is defined as

$$W_x^1[n,d] = \frac{w}{VN} \frac{(2m)^{\sum_y n_y - 2}}{(n_x - 1)!} \prod_{y \neq x} \frac{1}{n_y!} \cdots \tag{3.20}$$

where there is a *head* at some site x. The dimer weights hidden in the dots are exactly the same as in (3.17). We choose $w = 2(d-1) + 2t^2 + (2m)^2$ which may be understood as the possibilities the worm has to

propagate. In the following, we will see that this choice - together with the factor $1/VN$ - abolishes the need for accept-reject-steps.

First, we present the work flow of the worm. Afterwards, we proof detailed balance. Suppose, we take a configuration $C \in C^0$. With probability $1/V$ we pick a site x where we start the worm. Starting the worm means $C \to C' \in C^1$. This is possible in two ways: with probability n_x/N we label a monomer as *head*; with probability $d_{x,\nu}/N$ we put the head on an adjacent site $x+\hat{\nu}$. Note that for the site start there needs to be at least one monomer present, otherwise the probability for that move is simply 0. The second move is realized by decreasing the dimer occupation $d_{x,\nu}$ by 1 and increasing the monomer number at x by 1. At site $x+\hat{\nu}$ the Grassmann constraint is then satisfied with the *head*. Note that $(n_x + \sum_\nu d_{x,\nu})/N = 1$, meaning the worm always starts. At this and any other point in the Markov chain, we have two options: terminating the worm, i.e., $C' \to \tilde{C} \in C^0$, or moving the *head*, i.e., $C' \to C'' \in C^1$. With probability $(2m)^2/w$ we decide to terminate the worm by transforming the *head* into a monomer. We move the *head* with probability $1/w$ in directions $\nu = \pm 1, \pm 2, \ldots, \pm(d-1)$ and with t^2/w in directions $\nu = \pm d$. Note that $((2m)^2 + 2(d-1) + 2t^2)/w = 1$. Moving the head is again split into two possibilities: with probability $n_{x+\hat{\nu}}/(N - d_{x,\nu})$ we terminate the worm at the adjacent site $x+\hat{\nu}$; with probability $d_{x+\hat{\nu},\mu}/(N-d_{x,\nu})$ we move the head to a next-to-nearest site $x+\hat{\nu}+\hat{\mu}$ where no backtracking is allowed, i.e., $\mu \neq -\nu$. Note that $(n_{x+\hat{\nu}} + \sum_{\mu \neq -\nu} d_{x+\hat{\nu},\mu})/(N-d_{x,\nu}) = 1$. Lastly, we need to specify the action of the moving-terminating and moving-moving steps. Terminating the worm on the adjacent site $x+\hat{\nu}$ is realized by increasing the dimer occupation $d_{x,\nu}$ by 1 and decreasing the monomer occupation $n_{x+\hat{\nu}}$ by 1. Moving the *head* to the next-to-nearest site $x+\hat{\nu}+\hat{\mu}$ results again in increasing the dimer occupation $d_{x,\nu}$ by 1 and decreasing the dimer occupation $d_{x+\hat{\nu},\mu}$ by 1.
Let us comment on the *tail*: For $m \neq 0$ each monomer is considered as a *tail*, meaning that the worm may exit any time it encounters a monomer occupation different from 0. For the chiral limit, however, starting the worm is only possible on a link by introducing a monomer and a *head*. Of course, then the worm needs to close to terminate. For non-zero mass this is not true. Thus, by combining the various starting/terminating steps the worm can rearrange the monomer occupation, or alter the total monomer number in units of 2. On the other hand, the dimer content is shuffled by moving the worm.

To show the correctness of the approach, we prove that each step described above satisfies the detailed balance condition $P[C \to C']W[C] = P[C' \to C]W[C']$. In the following, we organize the detailed balance conditions as follows: Expressions written in square brackets, i.e., [and], indicate weights of the respective configurations. Expressions outside of the brackets indicate probabilities.

We start with the starting move where we introduce the *head* at a site x. The corresponding move would be the closing step at the same site. We write

$$\frac{1}{V}\frac{n_x}{N}\left[\frac{(2m)^{\sum_y n_y}}{n_x!}\right] = \frac{(2m)^2}{w}\left[\frac{w}{VN}\frac{(2m)^{\sum_y n_y - 2}}{(n_x-1)!}\right]. \tag{3.21}$$

The second starting step is the start on a link (x,ν). The change is reversed by the terminating step on the same link. Additionally, we define $t_\nu^2 = t^{2\delta_{\nu,\pm d}}$. For those moves the detailed balance equation is given by

$$\frac{1}{V}\frac{d_{x,\nu}}{N}\left[\frac{(2m)^{\sum_y n_y}}{n_x! n_{x+\hat{\nu}}!}\frac{(N-d_{x,\nu})!}{d_{x,\nu}!}t_\nu^2\right] = \frac{t_\nu^2}{w}\frac{n_x+1}{N-d_{x,\nu}+1}\left[\frac{w}{VN}\frac{(2m)^{\sum_y n_y}}{(n_x+1)! n_{x+\hat{\nu}}!}\frac{(N-d_{x,\nu}+1)!}{(d_{x,\nu}-1)!}\right]. \tag{3.22}$$

The composition of the l.h.s. should be obvious. For the r.h.s. we need to be careful: The action of starting the worm is $d_{x,\nu}-1$, n_x+1 and $n_{x+\hat{\nu}}$+*head*. To satisfy the Grassmann constraint, also the *head* is monomer valued. Thus, the monomer occupation at the respective site is $n_{x+\hat{\nu}}+1$. However, the weight of that *worm sector* configuration is given by (3.20).

The last ingredient of the algorithm is the moving step. This is by far the most complicated case since we need to consider two links simultaneously.

$$\frac{t_\nu^2}{w}\frac{d_{x+\hat{\nu},\mu}}{N-d_{x,\nu}}\left[\frac{w}{NV}\frac{(2m)^{\sum_y n_y-2}}{(n_x-1)!n_{x+\hat{\nu}+\hat{\mu}}!}\frac{(N-d_{x,\nu})!}{d_{x,\nu}!}\frac{(N-d_{x+\hat{\nu},\mu})!}{d_{x+\hat{\nu},\mu}!}t_\mu^2\right] = \frac{t_\mu^2}{w}\frac{d_{x,\mu}+1}{N-d_{x+\hat{\nu},\mu}+1}\left[\frac{w}{NV}\frac{(2m)^{\sum_y n_y-2}}{(n_x-1)!n_{x+\hat{\nu}+\hat{\mu}}!}\frac{(N-d_{x,\nu}-1)!}{(d_{x,\nu}+1)!}\frac{(N-d_{x+\hat{\nu},\mu}+1)!}{(d_{x+\hat{\nu},\mu}-1)!}t_\nu^2\right] \tag{3.23}$$

The first two expressions in the first line represent the probability to move from the site x to the next-to-nearest site $x+\hat{\nu}+\hat{\mu}$ as described above. The weight for some local C^1 configuration is then given in the brackets where the *head* sits on the site x. In the second line, we have the probability to move from $x+\hat{\nu}+\hat{\mu}$ back to x. We need to be careful since (i) the *head* moved (it sits now at $x+\hat{\nu}+\hat{\mu}$) and (ii) the dimer configuration changed. The dimer occupation at the link attaching to x got increased by 1 and the dimer occupation on the link attaching to $x+\hat{\nu}+\hat{\mu}$ got decreased by 1. Since n_x also includes the monomer we call *head,* the factor $(n_x-1)!$ in the r.h.s. arises from the fact that we move the *head* and, thus, need to lower the monomer number. Consequently, we obtain a factor of $((n_{x+\hat{\nu}+\hat{\mu}}+1)-1)!$ for the *head*. The factors for the dimers are straightforward. This completes our proof of detailed balance.

3.2.3 Observables

Consider the definition of the condensate. Instead of averaging over all possibilities to put $\overline{\psi}_x\psi_x$, we consider only some site x

$$\langle\overline{\psi}_x\psi_x\rangle = \frac{1}{Z_{C^0}}\sum_{\{n,b\}\in C^0}\frac{(2m)^{\sum_y n_y-1}}{(n_x-1)!}\prod_{y\neq x}\frac{1}{n_y!}\ldots, \tag{3.24}$$

where Z_{C^0} denotes the partition sum (3.17). Our algorithm, however, samples configurations according to the weights given in (3.20). Thus, we can write (3.24) as

$$\langle\overline{\psi}_x\psi_x\rangle = \frac{NV(2m)}{w}\frac{1}{Z_{C^0}}\sum_{\{n,b\}\in C^1}W_x^1[n,b]. \tag{3.25}$$

Furthermore, we can sum over all sites x (and divide by the volume). Then, it is possible to argue that

$$\langle\overline{\psi}\psi\rangle = \frac{Nm}{w}\langle L\rangle, \tag{3.26}$$

where L is the length of the worm. The latter is simply a measure for the number of C^1 configurations, i.e., configurations contributing to the condensate, that are generated in one update. As argued in [15], it is also possible to measure the chiral susceptibility. Including also a non-zero m yields

$$\chi_{\overline{\psi}\psi} = \frac{N}{w}\left(\sum_x n_x + 1 - \frac{2m^2}{w}\right)\langle L\rangle, \tag{3.27}$$

which corresponds to a definition of the susceptibility of $\chi_{\overline{\psi}\psi} = \partial\langle\overline{\psi}\psi\rangle/\partial(2m) + V\langle\overline{\psi}\psi\rangle^2$. The latter includes connected and disconnected terms.

3.2.4 Reweighting to SU(3)

Since the worm only measures U(3) expectation values, we need a strategy to reweight to SU(3). Above, we mentioned the strategy which we will use for measuring the observables. The SU(3) condensate is given by

$$\langle\overline{\psi}\psi\rangle_{SU(3)} = \frac{Nm}{w}\frac{\langle L'\rangle_{U(3)}}{\left\langle \prod_\ell [1+f_\ell(t)\mathrm{sign}(\ell)]\right\rangle_{U(3)}}, \tag{3.28}$$

where $L' = \sum_{i=1}^{L}\prod_{\ell_i}[1+f_{\ell_i}(t)\mathrm{sign}(t)]$. L is again the length of the loop which is equivalent to the number of C^1 configurations. Therefore, for each configuration the worm generates we need to calculate the product over all closed contours ℓ_i where each ...-1-2-1-… dimer chain is paired with a fermion loop. For the susceptibility we need to apply the same strategy.

3.2.5 Baryon bags

The concept of baryon bags has been proposed by Gattringer in [33]. As the name suggests, baryon bags are a combination of the worldline representation presented above and the concept of fermion bags. While in purely fermionic models, as shown at the beginning of this chapter, the bags arise naturally from the Grassmann nature of the fermion fields and the specific type of interaction, we need to invest some work to uncover the composite fermion fields, i.e., the baryons, in strong coupling QCD.

Let us start by expanding the Boltzmann factor in (3.7) in a power series, i.e.,

$$\begin{aligned} e^{S_F[\overline{\psi},\psi,U]} = \prod_x \sum_{n_x=0}^{3} \frac{(2m\overline{\psi}_x\psi_x)^{n_x}}{n_x!}\times \\ \prod_{x,\mu}\sum_{k_{x,\mu}=0}^{3}\frac{(\xi_{x,\mu}\overline{\psi}_x U_{x,\mu}\psi_{x+\hat{\mu}})^{k_{x,\mu}}}{k_{x,\mu}!}\times \\ \prod_{x,\mu}\sum_{\overline{k}_{x,\mu}=0}^{3}\frac{(-\xi_{x,\mu}\overline{\psi}_{x+\hat{\mu}}U^\dagger_{x,\mu}\psi_x)^{\overline{k}_{x,\mu}}}{\overline{k}_{x,\mu}!}. \end{aligned} \tag{3.29}$$

Since the Grassmann variables are 3-component vectors the expansions terminate at the third order. Following the expansion, we can use the Grassmann nature of the fermion field to separate the baryonic degrees of freedom from the monomials of lower order. First, we notice that the expansion of a local Boltzmann factor may be written as

$$\sum_{k=0}^{3}\frac{(\overline{\psi}U\psi)^k}{k!} = e^{\frac{(\overline{\psi}U\psi)^3}{3!}}\sum_{k=0}^{2}\frac{(\overline{\psi}U\psi)^k}{k!}. \tag{3.30}$$

Due to the SU(3) nature of the gauge links, it is possible to show that $(\overline{\psi}U\psi)^3 = (\overline{\psi}\psi)^3 = 3!\overline{B}B$. The latter symbol defines the composite baryon fields $B = \psi_1\psi_2\psi_3$ and $\overline{B} = \overline{\psi}_3\overline{\psi}_2\overline{\psi}_1$. Applying the latter also to the backward hopping term and (trivially) to the mass term yields

$$e^{S_F[\overline{\psi},\psi,U]} = e^{S_B[\overline{B},B]}\prod_x\sum_{n_x=0}^{2}\frac{(2m\overline{\psi}_x\psi_x)^{n_x}}{n_x!}\times$$

$$\prod_{x,\mu}\sum_{k_{x,\mu}=0}^{2}\frac{(\xi_{x,\mu}\overline{\psi}_x U_{x,\mu}\psi_{x+\hat{\mu}})^{k_{x,\mu}}}{k_{x,\mu}!}\times \prod_{x,\mu}\sum_{\overline{k}_{x,\mu}=0}^{2}\frac{(-\xi_{x,\mu}\overline{\psi}_{x+\hat{\mu}}U^{\dagger}_{x,\mu}\psi_x)^{\overline{k}_{x,\mu}}}{\overline{k}_{x,\mu}!}. \tag{3.31}$$

We collected all baryon terms in $S_B[\overline{B},B]$ which takes the form of a free staggered action of a 1-component composite field, i.e.,

$$S_B[\overline{B},B]=\sum_x 2M\overline{B}_xB_x+\sum_{x,\mu}\xi^3_{x,\mu}(\overline{B}_xB_{x+\hat{\mu}}-\overline{B}_{x+\hat{\mu}}B_x), \tag{3.32}$$

where $M=4m^3$ is the bare baryon mass and $\xi^3_{x,\mu}=\gamma_{x,\mu}t^{3\delta_{\mu,\pm d}}$. Suggestively, we denote $S_B[\overline{B},B]$ as the free baryon action. We stress that the separation of baryon and quark/di-quark, i.e., meson, terms in the fermion action holds for any value of β. However, the strong coupling limit drastically simplifies the gauge integrals, as shown below.
Now, we integrate out the gauge links. Due to $\int \mathrm{d}g f(g)=\int \mathrm{d}g f(g^{-1})$, where $g\in$ SU(N), the only non-vanishing contributions stem from the case $k_{x,\mu}=\overline{k}_{x,\mu}$. The remaining Grassmann integral takes the form

$$Z=\int\mathcal{D}[\overline{\psi}\psi]e^{S_B[\overline{B},B]}\prod_x\sum_{n_x=0}^{2}\frac{(2m\overline{\psi}_x\psi_x)^{n_x}}{n_x!}\prod_{x,\nu}\sum_{k_{x,\mu}=0}^{2}\frac{(3-k_{x,\mu})!}{3!k_{x,\mu}!}(\overline{\psi}_x\psi_x\overline{\psi}_{x+\hat{\mu}}\psi_{x+\hat{\mu}})^{k_{x,\nu}}. \tag{3.33}$$

Finally, it is possible to integrate out the Grassmann variables. To do so, we notice that baryonic terms described by the baryon action trivially saturate the Grassmann intergral (3.33) since $\overline{B}_xB_x$ contains all three colors. Thus, at strong coupling baryonic and mesonic degrees of freedom do not mix and can be integrated out separately. Therefore, we split the Grassmann measure into two disconnected domains: The bag region $\mathcal{B}$, and the complementary domain $\overline{\mathcal{B}}=\Lambda\setminus\mathcal{B}$ which is filled with mesonic degrees of freedom. More specifically, the bag region is a union of potentially disconnected baryon bags $\mathcal{B}_i$, i.e., $\mathcal{B}=\cup_i\mathcal{B}_i$, where the physics is described by $S_B[\overline{B},B]$. The Grassmann measure factorizes in the following way

$$\int\mathcal{D}[\overline{\psi}\psi]=\prod_i\int_{\mathcal{B}_i}\mathcal{D}[\overline{\psi}\psi]\ \times\ \int_{\overline{\mathcal{B}}}\mathcal{D}[\overline{\psi}\psi]. \tag{3.34}$$

The decomposition simplifies the strong coupling partition sum (3.33) to

$$Z=\sum_{\{\mathcal{B}\}}\left(\prod_{\mathcal{B}_i\in\mathcal{B}}Z_{\mathcal{B}_i}\right)\ \times\ Z_{\overline{\mathcal{B}}}, \tag{3.35}$$

where $\sum_{\{\mathcal{B}\}}$ is understood as a sum over all possible bag configurations on the lattice Λ. The integration over each individual baryon bag $\mathcal{B}_i$ yields the bag partition sum

$$Z_{\mathcal{B}_i}=\int\prod_{x\in\mathcal{B}_i}\mathrm{d}B_x\mathrm{d}\overline{B}_x\exp\Big(\sum_{x,y\in\mathcal{B}_i}\overline{B}_xD^{(i)}_{x,y}B_y\Big)=\det D^{(i)}, \tag{3.36}$$

where $D^{(i)}$ is the Dirac operator defined by the free staggered baryon action (3.32) restricted to the bag $\mathcal{B}_i$. Since the weight for each bag is just the fermion determinant of a free staggered Dirac operator, all weights are real and non-negative; at least for small chemical potential. Thus, for vanishing or small μ the fermion sign problem is solved completely.

Finally, we need to discuss the degrees of freedom occupying the complementary domain and the partition sum describing this subsystem, respectively. This domain is filled with quark and di-quark monomers n_x and dimers $k_{x,\mu}$, and the partition sum is given by [33,34]

$$Z_{\overline{\mathcal{B}}} = \sum_{\{n,k||\mathcal{B}\}} \prod_{x\in\overline{\mathcal{B}}} \frac{3!}{n_x!}(2m)^{n_x} \prod_{(x,\mu)\in\overline{\mathcal{B}}} \frac{(3-k_{x,\mu})!}{3!k_{x,\mu}!} t^{2k_{x,\mu}\delta_{\mu,\pm d}}, \tag{3.37}$$

where we introduced the sum over $\overline{\mathcal{B}}$ configurations. It is defined as

$$\sum_{\{n,k||\mathcal{B}\}} = \prod_{x\in\overline{\mathcal{B}}} \sum_{n_x=0}^{2} \prod_{(x,\mu)\in\overline{\mathcal{B}}} \sum_{k_{x,\mu}=0}^{2}. \tag{3.38}$$

At the end of this section, we would like to point out the differences to the worldline representation proposed by Karsch and Mütter [24]. If we would evaluate the fermion determinants in terms of worldlines, i.e., expanding the Boltzmann factor in (3.36) and integrating out the Grassmann variables in each bag, then the representation is identical to the latter: The baryon loops and tri-quark monomers and dimers occupy $\mathcal{B}$, quark and di-quark monomers and dimers $\overline{\mathcal{B}}$. This means the baryon bags simply sum up large sets of configurations in the Karsch-Mütter representation. But the resummation is executed in such a way that for $\mu = 0$ all weights are real and non-negative. Thus, simulating the system in the bag representation fully takes into account the SU(3) nature and reweighting is not necessary.

3.2.6 Updates

In contrast to the worldline system where we used a worm algorithm, we here use a local algorithm to update the bag system. This choice, however, prevents us from taking the chiral limit. The reason for this failure of the algorithm is that it tries to exchange a dimer with two monomers and vice versa. Since the acceptance rate for introducing a pair of monomers is $\rho \propto m^2$, the algorithm simply stops being ergodic once $m \ll 1$. Nonetheless, we use the local algorithm for a proof-of-concept study. For a clean description of the algorithm, we distinguish $\overline{\mathcal{B}}$-updates which shuffle the degrees of freedom in the complementary domain and $\mathcal{B}$-updates which change the bag domain.

Let us begin with the updates of the complementary domain. At some link (x,μ) we propose to change the dimer occupation $k_{x,\mu}$ by $\Delta k = \pm 1$. Consequently, we need to meet the Grassmann constraint by changing the monomer occupations n_x and $n_{x+\hat{\mu}}$ by $\Delta n = \mp 1$. But we only allow moves that do not produce tri-quark monomers and dimers. These moves are accepted with probability $\min(1, \rho_{\overline{\mathcal{B}}})$, where the accept-reject-rate is given by

$$\rho_{\overline{\mathcal{B}}} = \frac{n_x!}{n'_x!}\frac{n_{x+\hat{\mu}}!}{n'_{x+\hat{\mu}}!}(2m)^{2\Delta n}\frac{(3-k'_{x,\mu})!}{(3-k_{x,\mu})!}\frac{k_{x,\mu}!}{k'_{x,\mu}!}t^{2\Delta k\delta_{\mu,\pm d}}. \tag{3.39}$$

The change of the bag domain is by far more complex. On the one hand, bags need to grow and shrink, and, on the other hand, bags may also merge or split or develop holes. Thus, we need to be more careful here. All moves that change the bag domain automatically enlarge or diminish the size of the complementary domain. Thus, each $\mathcal{B}$-update will also include a factor similar to (3.39) which we denote as $\widetilde{\rho}_{\overline{\mathcal{B}}}$. The full accept-reject-ratio for a bag update is then given by

$$\rho_{\mathcal{B}} = \widetilde{\rho}_{\overline{\mathcal{B}}} \times \frac{\det D^{(i_1)\prime} \ldots \det D^{(i_n)\prime}}{\det D^{(i_1)} \ldots \det D^{(i_m)}}, \tag{3.40}$$

where we included the possibility that a move changes more than one bag. For example, in two dimensions it is possible to split a fractal bag with one move into two or three smaller bags.

The simplest cases are the growing and shrinking of a bag without changing the connectivity to other bags, i.e., without merging or splitting. On a practical level, we scan the region $\overline{\mathcal{B}}$ and the algorithm detects sites that can be added/removed to/from $\overline{\mathcal{B}}$, e.g., a site which is occupied by two monomers and is the endpoint of a dimer. Replacing this dimer by two monomers would produce a tri-quark monomer and, thus, this site belongs to $\mathcal{B}$. This means, we either propose to create a 1-site bag or grow a bag by one site. For growing a bag, the bag Dirac operator for the modified bag can be related to the old bag via

$$D^{(i)\,\prime} = \begin{bmatrix} D^{(i)} & H \\ -H^T & 8m^3 \end{bmatrix}, \tag{3.41}$$

where $D^{(i)}$ is the Dirac matrix of the unchanged bag, H is a vector that includes the off-diagonal terms (this encodes the connectivity of the site to the rest of the bag; in a way, it tells the system how many additional sites and links the new bag has), and $8m^3$ is simply the diagonal term of the modified Dirac matrix. Since $D^{(i)}$ is a square matrix and invertible, we employ a well-known relation to evaluate the determinant, i.e.,

$$\det \begin{bmatrix} A & B \\ C & D \end{bmatrix} = \det A \, \left(D - CA^{-1}B\right),$$

where A and D are square matrices and A is invertible. Thus, for a adding a single site the accept-reject-ratio is given by

$$\widetilde{\rho}_{\overline{\mathcal{B}}} \, \times \, \left(8m^3 + H^T D^{(i)\,-1} H\right). \tag{3.42}$$

Furthermore, (3.42) can be generalized to cases where adding a site to $\mathcal{B}$ merges multiple bags which we denote as $\mathcal{B}_{i_1}, \, \ldots \, \mathcal{B}_{i_k}$. The accept-reject-ratio for this class of moves is given by

$$\widetilde{\rho}_{\overline{\mathcal{B}}} \, \times \, \left(8m^3 + H_k^T D^{(i_1 \, \ldots \, i_k)\,-1} H_k\right), \tag{3.43}$$

where $D^{(i_1 \, \ldots \, i_k)\,-1} = \mathrm{diag}\left[D^{(i_1)\,-1}, \ldots, D^{(i_k)\,-1}\right]$ and $H_k^T = (H_{i_1}^T, \ldots, H_{i_k}^T)$ which include the hopping terms from the site into the various arms of the merged bag.
Secondly, we can shrink the bag region by removing a site from it. This results in deleting/shrinking a single bag or splitting multiple bags. As it turns out, the accept-reject-ratios for both cases have the same structure. We show the construction for a single bag where we cut away a single site. The bag determinant for the new bag reads

$$\det D^{(i)\,\prime} = \int \prod_{x \in \mathcal{B}_i'} \mathrm{d}B_x \mathrm{d}\overline{B}_x \exp\left(\sum_{x,y \in \mathcal{B}_i'} \overline{B}_x D_{xy}^{(i)\,\prime} B_y\right), \tag{3.44}$$

where $\mathcal{B}_i'$ is obtained from $\mathcal{B}_i$ by removing the site z. Using properties of the Grassmann numbers and the Grassmann integral, we find from (3.44)

$$\det D^{(i)\,\prime} = \int \prod_{x \in \mathcal{B}_i} \mathrm{d}B_x \mathrm{d}\overline{B}_x \, \overline{B}_z B_z \exp\left(\sum_{x,y \in \mathcal{B}_i} \overline{B}_x D_{xy}^{(i)} B_y\right) = \det D^{(i)} \, D_{zz}^{(i)\,-1}. \tag{3.45}$$

Note that we extended the integration domain to the old bag $\mathcal{B}_i$, and also the sum in the exponent runs over this domain. To correct for that, we insert by hand a bilinear $\overline{B}_z B_z$ which kills off all terms in the exponent that contain B_z or $\overline{B}_z$. For the last equal sign, we employed the Wick theorem. With this finding the accept-reject-ratio assumes an elegant form

$$\rho_{\overline{\mathcal{B}}} \times D^{(i)\,-1}_{zz}. \tag{3.46}$$

Note that the same construction can be used for the case where the removal of z yields two or more smaller bags.
For the algorithm to be ergodic, we need to include a move where we propose to change an isolated object containing two sites, e.g., two adjacent sites that both are occupied by one monomer and the link connecting both sites is occupied by a di-quark dimer. Such a move is necessary to allow for the case that the lattice is completely occupied by a single bag. The calculation of the accept-reject-ratio can also be automatized, as shown above, but some modifications are needed. For adding two sites, i.e., this is in principle a 2-site bag, to the current bag structure, we need to compute

$$\widetilde{\rho}_{\overline{\mathcal{B}}} \times \det\left(8m^3 \mathbb{1}_{2\times 2} + H_k^T D^{(i_1 \ldots i_k)\,-1} H_k\right), \tag{3.47}$$

where the H_k^T is now a matrix containing the off-diagonal terms from the Dirac operator for two sites. For simultaneously removing two sites from a bag, we can use the same strategy as in (3.45) with the difference that we need to insert two bilinears, i.e., one for each site to be removed. In such a case, the Wick theorem yields

$$\rho_{\overline{\mathcal{B}}} \times \det \begin{bmatrix} D^{(i)\,-1}_{zz} & D^{(i)\,-1}_{z'z} \\ D^{(i)\,-1}_{zz'} & D^{(i)\,-1}_{z'z'} \end{bmatrix}, \tag{3.48}$$

where we propose to remove z and z' from the bag.
To conclude this section, we make some comments on the updating scheme and data structure we use. As explained above we separately update $\mathcal{B}$ and $\overline{\mathcal{B}}$. The latter we update by shuffling the worldline degrees of freedom within and do not change the size of the domain. The principle which we use to change the configurations is always replacing a dimer by two monomers and vice versa. In a sense, this also holds for updating the $\mathcal{B}$ domain. To update the latter, we (i) scan $\overline{\mathcal{B}}$ and detect single sites which can be used to create/delete/grow/shrink/merge/split bags and (ii) propose to simultaneously change two sites occupied by an isolated monomer-dimer object into a 2-site bag and vice versa which may also result in creating/deleting/growing/shrinking/merging/splitting of bags. We store the sites belonging to a bag in a list. When the bag grows, we simply append the list, if the bag shrinks, we delete the respective entry. When a move merges bags, we append the full list of the secondary bag to the primary bag. Crucially, however, is the splitting of a bag into smaller bags. For this case, we always need to check the connectivity of the remnant bags to ensure that the sites within those fragments are assigned to the correct bag. For each bag we store the inverse of the bag Dirac operator which is updated once the algorithm accepts a move to change a bag. This will also become handy when we consider the computation of the chiral condensate, as we will see in the next section.

3.2.7 Observables

To cross-check the results from the bag simulation, we consider the chiral condensate in the bag representation, i.e.,

$$\langle\overline{\psi}\psi\rangle = \frac{1}{V}\left\langle 3(2m)^2 \sum_i \mathrm{tr} D^{(i)\,-1} + \frac{\sum_{x\in\overline{\mathcal{B}}} n_x}{2m} \right\rangle, \tag{3.49}$$

where the expectation value $\langle \ldots \rangle$ is computed with respect to the bag partition sum (3.35). This observable, however, is merely of secondary interest. The primary observable we are interested in is the bag size σ_B. It is defined as

$$\sigma_B = \frac{1}{V}\sum_i |\mathcal{B}_i|, \tag{3.50}$$

where $|\mathcal{B}_i|$ is given by the number of sites in the bag $\mathcal{B}_i$. Therefore, σ_B signals the fraction of the lattice in which the physics can be described by the free baryon action (3.32). In the following, we are interested in studying this quantity as a function of the temperature, to see how the worldline degrees of freedom change when we approach the critical temperature of the chiral transition.
Note that also with the worm algorithm we are able to measure σ_B. Since the bags are not natural in this representation, this will require some workarounds. We know that the bag is filled with tri-quark monomers and dimers and loops. Thus, for each SU(3) worldline configuration we can uniquely identify the bag structure: σ_B is simply given by the number of sites occupied by $n_x = 3$, $d_{x,\mu} = 3$ and $\ell_{x,\mu} = \pm 1$. However, the worm simulates U(3), and we merely reweight to SU(3). So, the bag size may be measured with

$$\langle \sigma_B \rangle_{SU(3)} = \frac{1}{V} \frac{\left\langle \sigma_B \prod_\ell \left[1 + f_\ell(t) \mathrm{sign}(\ell)\right] \right\rangle_{U(3)}}{\left\langle \prod_\ell \left[1 + f_\ell(t) \mathrm{sign}(\ell)\right] \right\rangle_{U(3)}}. \tag{3.51}$$

What does the expression $\sigma_B \prod_\ell \left[1 + f_\ell(t) \mathrm{sign}(\ell)\right]$ precisely mean? Suppose we take any U(3) configuration. Some sites will be occupied by tri-quark monomers and dimers. This number of sites we denote as $\sigma_B^{(0)}$. Furthermore, we collect all closed contours of alternating quark and di-quark dimers and superpose those with baryon loops. Of course, the presence of baryon loops affects the total bag size σ_B. To make that evident, we write

$$\prod_\ell \left[1 + f_\ell(t) \mathrm{sign}(\ell)\right] = \prod_{\ell=1}^{L} \sum_{m_\ell=0}^{1} \left(f_\ell(t) \mathrm{sign}(\ell)\right)^{m_\ell}, \tag{3.52}$$

where $m_\ell = 0$ signals that the contour is viewed as a dimer chain and for $m_\ell = 1$ the contour is occupied by a baryon loop. L is the total number of closed contours. With the help of (3.52), we can now evaluate the bag size for a U(3) configuration,

$$\sigma_B \prod_\ell \left[1 + f_\ell(t) \mathrm{sign}(\ell)\right] = \sum_{\{m_\ell\}} \prod_{\ell=1}^{L} \left(f_\ell(t) \mathrm{sign}(\ell)\right)^{m_\ell} \sigma_B^{(\{m_\ell\})}, \tag{3.53}$$

where $\sigma_B^{(\{m_\ell\})} = \sigma_B^{(0)} +$ # sites occupied by active loops. To illustrate the procedure, we take a U(3) configuration where two plaquettes are occupied by closed chains of quark and di-quark dimers. We may call them ℓ_1 and ℓ_2. Additionally, some sites are occupied by two tri-quark dimers and a single 3-quark monomer. This yields $\sigma_B^{(0)} = 5$. With the current configurations, four cases are possibile: $m_{\ell_1} = 0$ and $m_{\ell_2} = 0$, $\sigma_B^{(\{m_\ell\})} = \sigma_B^{(0)} = 5$; $m_{\ell_1} = 1$ and $m_{\ell_2} = 0$, $\sigma_B^{(\{m_\ell\})} = \sigma_B^{(0)} + 4 = 9$; $m_{\ell_1} = 0$ and $m_{\ell_1} = 0$ $m_{\ell_2} = 1$, $\sigma_B^{(\{m_\ell\})} = 9$; $m_{\ell_1} = 1$ and $m_{\ell_2} = 1$, $\sigma_B^{(\{m_\ell\})} = 13$. The total bag size S_B of the example U(3) configuration then is

$$\sigma_B \prod_\ell \left[1 + f_\ell(t) \mathrm{sign}(\ell)\right] = 5 + 9(\pm f_{\ell_1}(t)) + 9(\pm f_{\ell_2}(t)) + 13(\pm f_{\ell_1}(t))(\pm f_{\ell_2}(t)),$$

where the ± 1 stem from the signs of the baryon loops. Thus, the sum $\sum_{\{m_\ell\}}$ contains 2^L terms. For small lattices this may be evaluated exactly, as shown above. On bigger lattices, however, a stochastic evaluation with simple sampling may be numerically less demanding.

3.2.8 Testing the algorithms

We test both the bag simulation and the worm on 2×2 and 4×4 lattices. The 2×2 case is appealing because in this case exact results can be computed. We also need to test the algorithms on a 4×4 lattice

since there configurations appear that are not allowed on a 2×2 lattice, e.g., multiple 1-site bags or a 3-site bag. On the 4×4 lattice, we cannot provide exact results, but we confront the condensate obtained by the worldline methods with data obtained by a conventional simulation. In particular, we are interested in thoroughly testing the bookkeeping algorithm of the bag simulation to ensure that the program reliably tracks the bags while they grow/shrink/merge/split. The last two moves, for example, do not appear on the 2×2 lattice.

We start with the 2×2 case. On the latter all configurations can be ordered in four classes according to the bag configuration: no bags, one 1-site bag, one 2-site bag, one 4-site bag. For each class, we systematically count the possible $\overline{\mathcal{B}}$ configurations by hand. The total partition sum is given by

$$Z = \frac{1160}{9} + \frac{2560}{3}(2m)^2 + 1351(2m)^4 + 800(2m)^6 + 208(2m)^8 + 24(2m)^{10} + (2m)^{12}. \quad (3.54)$$

From the latter the chiral condensate $\langle\overline{\psi}\psi\rangle$ and susceptibility $\chi_{\overline{\psi}\psi}$ may be computed. To obtain the bag size σ_B, one actually needs to consider the partition sums for each class individually. Each partition sum is then weighted by the number of sites in the bag and divided by (3.54). See the left panel of Figure 3 for results obtained on the 2×2 lattice.

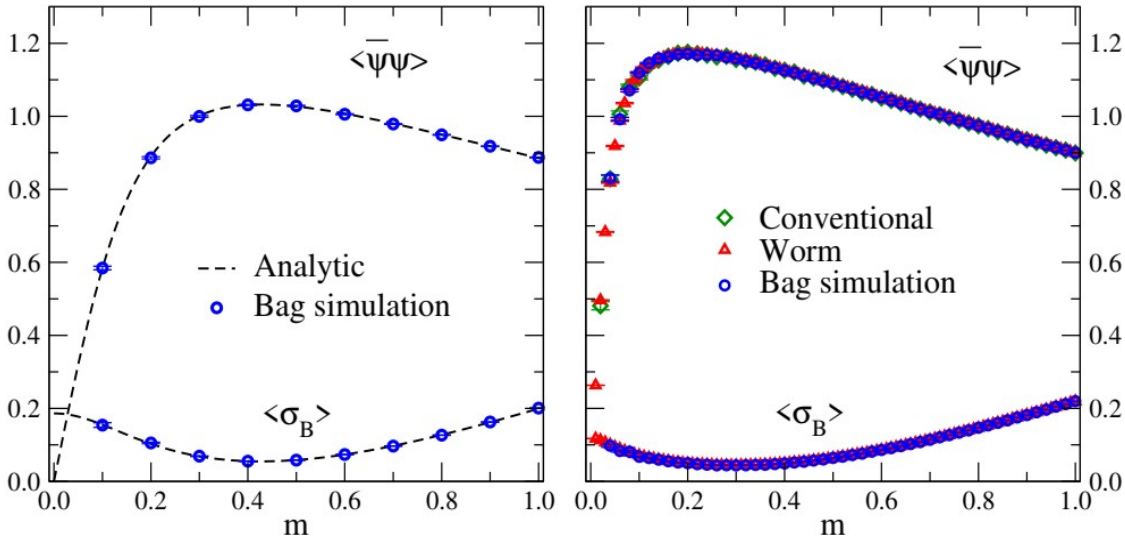

Figure 3: Cross-checks for the bag and worm simulations. The observables are the chiral condensate $\langle\overline{\psi}\psi\rangle$ and the bag size $\langle\sigma_B\rangle$. Lhs.: $V = 2 \times 2$, blue circles denotes data obtained from a worldline simulation using the bag representation. The dashed line is the analytic result obtained by systematically counting configurations. Rhs.: $V = 4 \times 4$, blue circles are again computed with a bag simulation. The red triangles are data points obtained by a worm simulation. The green diamonds stem from a conventional simulation using fermion determinants and provide an additional cross-check.

For the 4×4 case, we compare the results from the bag simulation with the data from worm simulation. Additionally, we compute the chiral condensate with a conventional simulation using only the fermion determinant as a weight factor to confront the worldline results. The gauge field is sampled with a simple local Metropolis algorithm. See the right panel of Figure 3 for the respective results. We would like to point out that the range of m is different for the bag and worm simulations. The reason for this is, as explained before, that the local algorithm used for the bag simulation is inefficient for small values of m.
We clearly see that in both cases the data from the worldline simulation match the reference data within error bars and conclude that both simulations have been implemented correctly. In the next section, we show numerical results for larger system sizes. Before we proceed, we would like to comment on the

algorithm that we are going to use in the following: Since the local algorithm used for updating the system in the bag representation is bad for the interesting small m region, we are going to use the worm simulation to obtain data on larger lattices.

3.3 Results

In the following, as a proof-of-concept study, we explore the $\mu = 0$ line in the T-μ phase diagram of strong coupling QCD in two dimensions. The results shown below are computed on a $V = 4 \times N_s$ lattice where the temperature is varied by adjusting the bare anisotropic coupling t. In this work, we are interested in a qualitative study. Thus, we refrain from determining the temperature associated with a given t. We merely stress that the temperature T is strictly increasing with t [35]. For non-vanishing m we choose $N_s = 16$, and for the case of vanishing quark mass we vary $N_s = 8, 12, ...24$ to see a potential scaling of the susceptibility. As explained above, we only use the worm algorithm. We use 10^4 worms to equilibrate the system. Subsequently, we measure the observables 10^6 times separated by 10 worms for decorrelation. The plots are organized in such a way that we always show a canonical observable, such as the condensate or the susceptibility, in comparison to the bag size. The reason for this is that we are interested in the correlations between the change in the canonical observables and the worldline degrees of freedom, signaled by the bag size.

In Figure 4, we show the condensate (top plot) and the bag size (bottom plot) as function of m for various values of the anisotropy t. Due to the definition of the condensate given by Equation (3.26), the condensate exactly vanishes for $m = 0$. If we increase the quark mass, we allow that sites get populated by monomers. This results in a rapid increase of the condensate (compare with Equation (3.19) where m appears in the

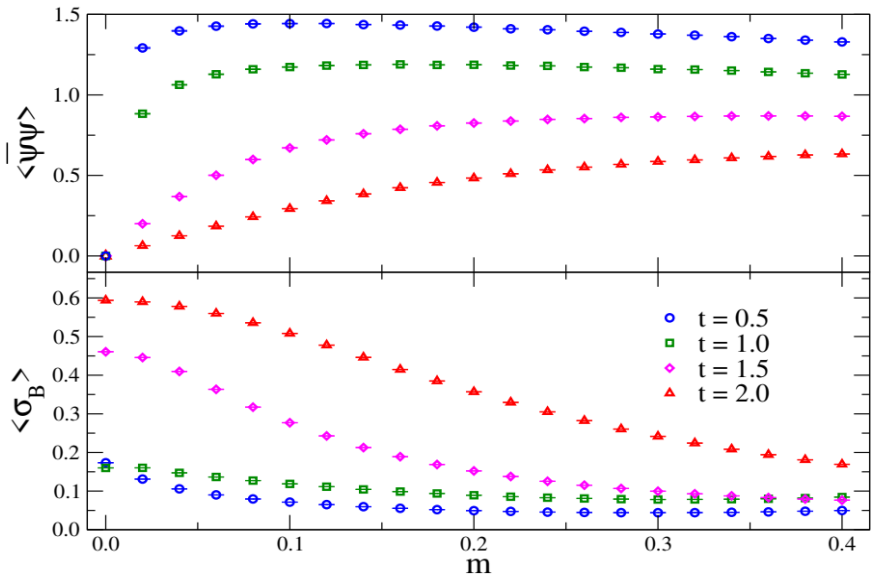

Figure 4: The chiral condensate $\langle\overline{\psi}\psi\rangle$ (top) and the bag size $\langle\sigma_B\rangle$ (bottom) for various t as a function of the bare quark mass m. The results were obtained on a $V = 4 \times 16$ lattice.

denominator). For larger values of the anisotropy t (i.e., higher temperatures), dimers are favored, and, thus, the increase of the condensate is weakened. Interestingly, the variation of the condensate is accompanied by a corresponding variation in the expectation value of the bag size. Also, it seems that the average bag size responds differently to a change in the quark mass depending on the value of the anisotropy t. This will become clear when we fix m and drive the bare anisotropic coupling t.

Figure 5 shows the chiral condensate (top) and the average bag size (bottom) as a function of the anisotropy t for fixed quark mass. We observe two regions that seem to have different response to a change in the quark mass. In a future work, we plan to address this aspect [36].

Since the condensate vanishes in the chiral limit, we show a separate plot for this case. Figure 6 shows the chiral susceptibility (top) and the average bag size (bottom) as a function of the anisotropy t for various

spatial lattice extents N_s. Clearly, we see that a change of the scaling behavior occurs when t is increased. This hints torwards a change of phase. The phase structure of a two-dimensional system was discussed in [15]. The argument is the following: Since chiral symmetry cannot be broken spontaneously in two dimensions, the system is in a critical massless phase where the susceptibility scales with the system size. When the anisotropy t is increased the scaling is smoothly diminished and eventually vanishes. Then, the system is in the symmetric phase where the fermionic degrees of freedom (signaled by σ_B) seem to be dominant. Also, the nature of the scaling, in particular the t-dependence and the connection to the bag size, will be quantified in a future publication [36].

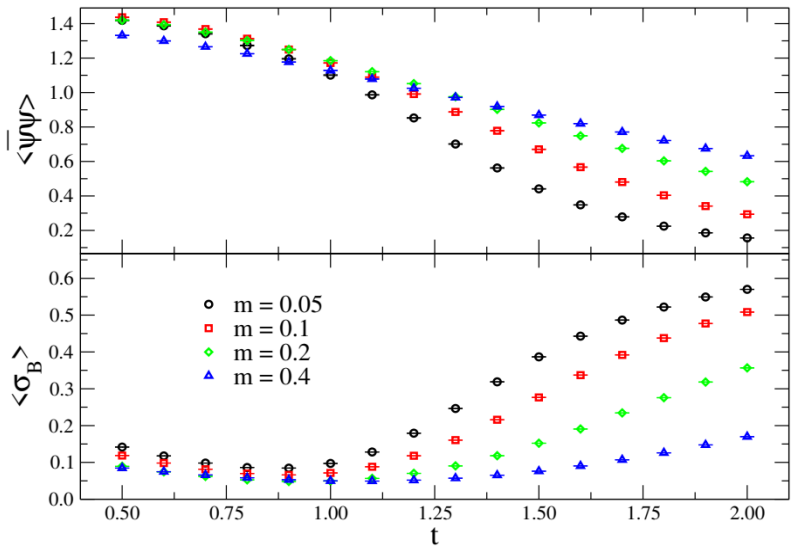

Figure 5: The chiral condensate $\langle\bar{\psi}\psi\rangle$ (top) and the bag size $\langle\sigma_B\rangle$ (bottom) for various values of the quark mass m as a function of the anisotropic coupling t. The results were obtained on a $V = 4 \times 16$ lattice.

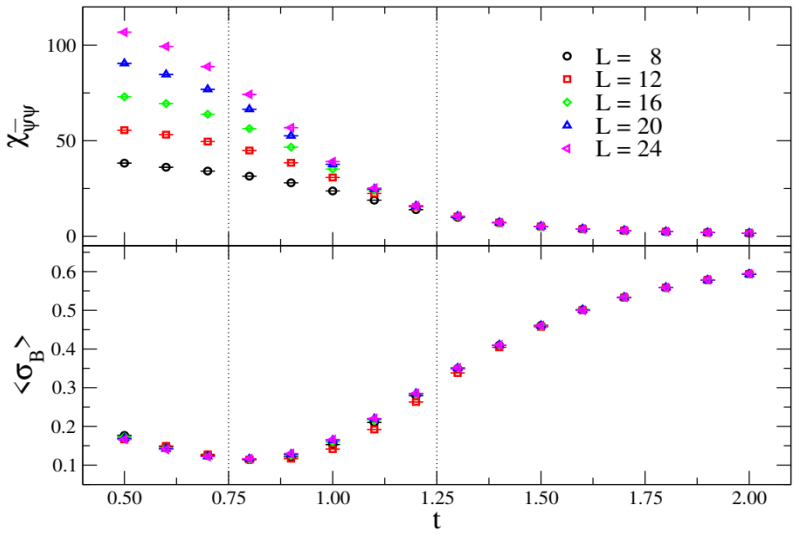

Figure 6: Chiral susceptibility $\chi_{\bar{\psi}\psi}$ (top) and bag size $\langle\sigma_B\rangle$ (bottom) as a function of the bare anisotropic coupling t. The results were obtained on a $V = 4 \times L$ lattice, where the spatial extent L is varied.

At the end, we would like to comment on an interesting detail: In Figure 6, the bag size seems to saturate at $2/3$ for large values of t. This can be understood in the following way: If we take $t \gg 1$, then the temporal links will be predominantly occupied. Locally, the partition sum will only contain six distinct objects: two baryon loop orientations, two possibilities for tri-quark dimers, and two possibilities for the mesonic dimer chain. However, for the bag we only count four of the objects, giving $2/3$ in total. This is because at $\mu = 0$ a loop and the corresponding dimer chain have the same weight in this limit. If we take the chemical potential to a non-zero value, then the forward-winding loops are favored, and we expect that $\langle \sigma_B \rangle$ approaches 1 instead.

3.4 Conclusions and Outlook

In the second part of this report, we showed recent progress in simulating strong coupling QCD in the baryon bag representation. Due the Grassmann nature of the fermion fields and the SU(3) nature of the gauge fields, it is possible to factorize the Boltzmann factor containing the fermion action into baryon (tri-quark) and meson (quark/di-quark) terms. Note that this factorization is not restricted to the strong coupling limit. The latter, however, simplifies the integrals tremendously: Taking the strong coupling limit completely separates domains that are occupied by baryons from domains occupied by the mesonic contributions. The baryons are confined in so-called baryon bags where the physics is described by a free staggered action of a 1-component composite field. The meson domain, on the other hand, is filled with networks of monomers and dimers. In this formulation the fermion sign problem is exactly solved since each bag has a weight which is given by the determinant of a free staggered Dirac matrix. The determinant superposes all possible worldline configurations compatible with a given domain, and, thus, for $\mu = 0$ all weights are real and non-negative.

Since baryons and mesons are completely separated an interesting question arises: What are the prevalent worldline degrees of freedom? To answer this we define a novel quantity which can only be motivated in the baryon bag approach: the bag size σ_B. Of course, every worldline configuration can be thought of as a bag configuration where one possible worldline occupation is chosen for the bags. Thus, also in the worldline representation introduced by Karsch and Mütter it is possible to measure the bag size. This advantage we use to cross-check the bag representation on small lattices and to obtain actual results on larger lattices. The reason for this workaround is the following: Due to the factorized nature (bags and complementary domain) of the bag system, it is not easy to define a worm algorithm. We postpone this endeavor and use a local algorithm for the cross-checks. This should be understood as a proof-of-principle and as a motivation to study the worldline degrees of freedom using the bag size. On the other hand, it is easier to develop a worm algorithm for a U(N) worldline system. A worm simulating the chiral limit of U(N) worldline models was already available [15], and, thus, we merely extended the latter to non-vanishing quark mass. Moreover, the algorithm is well tested and extremely efficient.

In order to show that the bag representation is correct, we provided two important cross-checks. On a 2×2 lattice we provided analytic results which can be obtained by systematically counting all possible configurations. For a cross-check on the second of the small lattices, i.e., 4×4, we confronted the data with results from the worm simulation and – for the condensate – from a conventional simulation. Both cross-checks showed perfect agreement of the methods. Since the worm is efficient and allows us to study the chiral limit, we exclusively use this strategy for simulations on larger lattices. In particular, we are interested in the response of the chiral condensate/susceptibility and the bag size with respect to a change in t and m. The bag size is an interesting quantity since it signals a change in the worldline degrees of freedom. In Figure 5 both the condensate and the bag size show interesting scaling with the quark mass m, whereas in Figure 6 the susceptibility shows scaling behavior with the system size that strongly depends on t. Interestingly, the bag size seems to be large when the susceptibility does not scale at all. Those aspects and the nature of the respective scaling will be addressed in a future publication [36].

For future studies, we plan to investigate the chiral transition in four dimension where chiral symmetry is restored in a second-order phase transition [25]. Furthermore, to avoid the bypass where we used the ordinary worldline representation and a reweighting strategy, we plan to develop a worm directly in the baryon bag representation.

4 Acknowledgments

First of all, I want to thank my advisor, Christof Gattringer, for his never-ending support and for encouraging me to go abroad. Also, I am indebted to my advisor at Duke University, Shailesh Chandrasekharan. I very much enjoyed our work and discussions on worldlines and algorithms. Additionally, I want to thank my colleagues at Duke, Hersh Singh, Hanqing Liu and Mendel Nguyen, who made my stay very pleasant. The friday-afternoon-seminars were informative and definitely contributed to broaden my scientific horizon. The burgers at Bull City afterwards were always hard-earned. A special thanks goes out to Mendel for our chats about coffee and politics and for taking me to Counter Culture!
Furthermore, I want to thank Duke University, in particular the Physics Department, for sponsoring my research stay and for the generous hospitality during my visit. Especially, I want to thank Cristin Ryman for all the help concerning the visa application process and other matters.
Also, I am grateful to Daniel Göschl for sending me the reference data shown in Chapter 2.
Last but not least, I want to thank the Austrian Marshall Plan Foundation for providing financial support to realize my stay at Duke University. My visit to the US was pleasant and instructive in every regard, scientifically as well as personally, and I will be eternally grateful for this unique experience.

5 Bibliography

[1] M. Troyer, U.-J. Wiese, Phys.Rev.Lett. 94, 170201 (2005)

[2] P. Hasenfratz, F. Karsch, Phys.Lett. 125B, 308 (1983)

[3] M. D'Elia, F. Negro, Phys.Rev.Lett. 109, 072001 (2012)

[4] P. Henelius, A. W. Sandvik, Phys. Rev. B 62, 1102 (2000)

[5] S. Chandrasekharan, PoS Lattice2008, 003 (2008)

[6] G. Aarts, PoS Lattice2009, 024 (2009)

[7] Z. Fodor, S.D. Katz, Phys.Lett. B 534, 87 (2002)

[8] P. de Forcrand, S. Kratochvila, Nucl.Phys.Proc.Suppl. 153, 62 (2006)

[9] K. Langfeld, B. Lucini, A. Rago, Phys.Rev.Lett. 109, 111601 (2012)

[10] N. D. Mermin, H. Wagner, Phys.Rev.Lett. 17, 1133 (1966)

[11] C. Gattringer, T. Kloiber, V. Sazonov, Nucl. Phys. B 897, 732 (2015)

[12] D. Göschl, C. Gattringer, A. Lehmann, C. Weis, Nucl. Phys. B 924, 63 (2017)

[13] P. W. Kasteleyn, Physica 27, 1209 (1961)

[14] S. Sharma, PoS LATTICE2018, 009 (2019)

[15] D. Adams, S. Chandrasekharan, Nucl. Phys. B 662, 220 (2003)

[16] S. Chandrasekharan, Phys.Rev. D 82, 025007 (2010)

[17] S. Chandrasekharan, A. Li, Phys.Rev. D 85, 091502 (2012)

[18] S. Chandrasekharan, Phys.Rev. D 86, 021701 (2012)

[19] S. Chandrasekharan, A. Li, Phys.Rev. D 88, 021701 (2013)

[20] E. Huffman, S. Chandrasekharan, Phys.Rev. B 89, 111101 (2014)

[21] E. Huffman, S. Chandrasekharan, PoS LATTICE2014, 058 (2014)

[22] E. Huffman, S. Chandrasekharan, Phys.Rev. E 94, 043311 (2016)

[23] C. Hann, E. Huffman, S. Chandrasekharan, Annals Phys. 376, 63 (2017)

[24] F. Karsch and K. H. Mütter, Nucl. Phys. B 313, 541 (1989)

[25] G. Boyd, J. Fingberg, F. Karsch, L. Karkkainen and B. Petersson, Nucl. Phys. B 376, 199 (1992)

[26] P. de Forcrand and M. Fromm, Phys. Rev. Lett. 104, 112005 (2010)

[27] P. de Forcrand, J. Langelage, O. Philipsen and W. Unger, Phys. Rev. Lett. 113, 152002 (2014)

[28] G. Gagliardi, J. Kim and W. Unger, EPJ Web Conf. 175, 07047 (2018)

[29] G. Gagliardi, W. Unger, PoS LATTICE2018, 224 (2018)

[30] M. Creutz, J. Math. Phys. 19, 2043 (1978)

[31] P. Rossi and U. Wolff, Nucl. Phys. B 248, 105 (1984)

[32] U. Wolff, Phys. Lett. 153B, 92 (1985)

[33] C. Gattringer, Phys.Rev. D 97, 074506 (2018)

[34] C. Marchis, C. Gattringer, O. Orasch, PoS LATTICE2018, 243 (2018)

[35] P. de Forcrand, W. Unger, Helvio Vairinhos, Phys.Rev. D97, 034512 (2018)

[36] O. Orasch, S. Chandrasekharan, C. Gattringer, work in preparation

[37] C. Gattringer, C. B. Lang, Lect. Notes Phys. 788 (2010)